A SUMMARY OF HINGELESS-ROTOR STRUCTURAL LOADS AND DYNAMICS RESEARCH

By John F. Ward

NASA Langley Research Center
Langley Station, Hampton, Va., U.S.A.

Presented at the Symposium on the Noise and Loading Actions on Helicopter V/STOL Aircraft and Ground Effect Machines

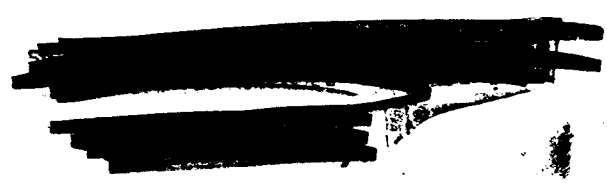

University of Southampton
Southampton, England
August 30 - September 3, 1965

A SUMMARY OF HINGELESS-ROTOR STRUCTURAL LOADS AND DYNAMICS RESEARCH

By John F. Ward*
NASA Langley Research Center

SUMMARY

This paper presents a summary of research programs dealing with helicopter hingeless-rotor structural loads and dynamics. The programs include (1) flight investigations, (2) dynamic-model wind-tunnel tests, and (3) derivation and substantiation of simplified analytical techniques for the prediction of critical structural loads in maneuver flight. Comparison of measured data and analytical results will be utilized in order to clarify the trends observed in the flight and wind-tunnel results.

INTRODUCTION

The purpose of this paper is to summarize some of the recent research activities dealing with helicopter hingeless-rotor structural loads and dynamics. This work includes flight-test, wind-tunnel investigations, and analytical studies. The interest in the hingeless rotor stems from the fact that it offers potential advantages in a number of areas. First, because of the cantilever action of the blades, large control moments can be developed and transferred directly from the rotor into the fuselage as a strong source of aircraft pitching and rolling moment. This results in order-of-magnitude improvements in the rotor control power and damping capability, which leads to significant improvements in the handling qualities of the helicopter. The second area of improvement stems from the opportunity to achieve a substantial reduction in rotor hub complexity with the elimination of the blade flapping and lagging hinges, in-plane blade dampers, and associated hardware. This reduction in complexity, which results in less mechanical maintenance, also provides an opportunity for a significant reduction in rotor hub drag.

While the cantilever rotor design is not new to the helicopter field, the current designs, in contrast to early "rigid" rotors, do not attempt to eliminate flexibility in the rotor system. It is believed that most and perhaps all of the past failures with the cantilever systems stemmed from attempts at preventing flexibility. The flexible hingeless-rotor system represents a new aeroelastic configuration and therefore requires a thorough investigation of the structural load and dynamic characteristics of the concept.

---

*Aerospace Technologist.

SYMBOLS

a	section lift-curve slope
B_1	lateral component of blade cyclic feathering motion, radians
C_T	thrust coefficient
c	blade chord, in.
e_v	virtual hinge offset, in.
I_v	mass moment of inertia about virtual hinge, slug-ft^2
K_{1F}	Southwell coefficient for first flapwise mode
K_{VF}	effective spring stiffness at virtual flapping hinge, in-lb/radian
K_{VL}	effective spring stiffness at virtual lag hinge, in-lb/radian
M_A	longitudinal component of rotor hub moment, in-lb
M_B	lateral component of rotor hub moment, in-lb
M_C	blade chordwise bending moment, in-lb
M_{VL}	moment about virtual lag hinge, in-lb
M_{tip}	tip Mach number
M_w	blade weight moment about root end, in-lb
p	aircraft rolling angular velocity, radians/sec
q	aircraft pitching angular velocity, radians/sec
R	blade radius, in.
t	time, sec
V	velocity along flight path, mph
V_{sim}	simulated full-scale velocity along flight path, mph
w_{1R}	blade first-mode flapwise deformation, rotating, in.

x	ratio of blade element radius to blade radius
β_1	amplitude of blade first harmonic flapping angle with respect to shaft axis, radians
Γ_1	amplification factor
Γ_L	lag response coefficient
γ	blade Lock number
γ_v	blade Lock number, based on virtual lag hinge, $\rho acR^4/I_v$
δ_1	damping coefficient in first mode
η	load factor
θ_o	blade collective pitch angle, radians
θ_1	first harmonic cyclic blade pitch, radians
θ_t	total blade twist, radian
μ	rotor tip speed ratio, $V/\Omega R$
ν_{1R}	blade first chordwise mode natural frequency, rotating, radian/sec
ν_{1S}	blade first chordwise mode natural frequency, nonrotating, radian/sec
ϵ_v	nondimensional offset of virtual hinge
ρ	density of atmosphere, slugs/ft^3
σ_v	blade first mass moment about virtual hinge, slug-ft
$\Phi_{\beta,1}$	azimuth phase angle of first harmonic blade flapping angle, degree
$\Phi_{\theta,1}$	azimuth phase angle of first harmonic blade cyclic feathering, degree
φ_c	azimuth phase angle of cyclic control input, degree
ψ	blade azimuth position, degree
Ω	rotor rotational speed, radians/sec
Ω_n	normal operating rotor rotational speed, radians/sec

ω_{1R} blade first flapwise mode natural frequency, rotating, radians/sec

ω_{1S} blade first flapwise mode natural frequency, nonrotating, radians/sec

GENERAL CHARACTERISTICS OF HINGELESS ROTOR

The hingeless rotor is sometimes referred to as a "rigid" rotor system. While this terminology focuses attention on the primary difference between hingeless and articulated rotors, it must be recognized that, in fact, it is the use of flexibility that is the key to the successful utilization of the hingeless-rotor concept. From the standpoint of structural loads and dynamics, the hingeless rotor represents a fundamental change from dealing with the articulated blade dynamic response in the rigid-body pendulum mode to dealing with the cantilever blade dynamic response in the first bending mode. Certainly a rigorous treatment of either configuration would deal with higher order bending modes, but it is the nature of the first-mode response characteristics that determines the fundamental differences in the two rotor systems.

Blade Flapping Response

A comparison of hinged and cantilever blade first-mode natural frequencies as a function of rotor speed is shown in figure 1. A curve of the first-mode natural frequency in the flapwise degree of freedom, as a function of rotor rotational speed, is given for each of three uniform blade configurations: (1) zero-offset hinged blade, (2) conventional offset hinged blade, and (3) a typical cantilever blade. Also shown are the first-mode shapes for the three configurations. The frequencies and mode shapes shown in figure 1 were obtained from reference 1. While the mode shapes for the hinged rigid-body modes are not influenced by rotational speed, the cantilever mode is altered somewhat by centrifugal stiffening, which reduces the curvature over the outboard portion of the blade.

From the standpoint of rotor control and response, the predominating force inputs are occurring at once-per-rotor revolution. A typical source of such once-per-revolution force inputs is the aerodynamic force resulting from rotor cyclic control. The governing equation of motion for the flapping degree of freedom response to cyclic control input in hovering flight is:

$$\frac{d^2\beta_1}{d\psi^2} + \frac{\gamma}{8}\left(\frac{4}{3}\frac{\int_0^1 x w_{1R}{}^2 dx}{\int_0^1 w_{1R}{}^2 dx}\right)\frac{d\beta_1}{d\psi} + \left(\frac{\omega_{1R}}{\Omega}\right)^2\beta_1 = \frac{\gamma}{8}\left(\frac{4}{3}\frac{\int_0^1 x^2 w_{1R}\, dx}{\int_0^1 w_{1R}{}^2 dx}\right)\theta_1 \sin\left(\Omega t - \phi_c\right) \tag{1}$$

$$\frac{\beta_1}{\theta_1} = \Gamma_1 \frac{\beta_{1,\text{static}}}{\theta_1} \tag{2}$$

$$\frac{\beta_{1,\text{static}}}{\theta_1} = \frac{\gamma}{8}\left(\frac{\Omega}{\omega_{1R}}\right)^2\left(\frac{4}{3}\frac{\int_0^1 x^2 w_{1R}\,dx}{\int_0^1 w_{1R}^2 dx}\right) \tag{3}$$

$$\Gamma_1 = \left\{\left[1 - \left(\frac{\Omega}{\omega_{1R}}\right)^2\right]^2 + 4\delta_1^2\left(\frac{\Omega}{\omega_{1R}}\right)^2\right\}^{-1/2} \tag{4}$$

$$\delta_1 = \frac{\gamma}{16}\left(\frac{\Omega}{\omega_{1R}}\right)\left(\frac{4}{3}\frac{\int_0^1 x w_{1R}^2 dx}{\int_0^1 w_{1R}^2 dx}\right) \tag{5}$$

$$\Phi_{\theta,1} = \tan^{-1}\left[\frac{2\delta_1\left(\frac{\Omega}{\omega_{1R}}\right)}{1 - \left(\frac{\Omega}{\omega_{1R}}\right)^2}\right] \tag{6}$$

Substitution of the natural frequencies ω_{1R} and mode shapes w_{1R} at normal operating rotor speed from figure 1 into the above equations will give the relative response characteristics of the hinged and cantilever blades. Assuming the blades are identical in uniform mass distribution and aerodynamic characteristics, the relative response characteristics are shown in figure 2. The three-blade configurations are being forced at a frequency at or slightly above their natural frequency and the results indicate that the relative amplitude responses of the three blades are very nearly the same. Therefore, the cantilever rotor blade deforms like a hinged blade and is far from being a structurally "rigid" blade.

In the case of the phase response of the three blade types, it can be seen in figure 2 that the cantilever blade phase response is quite different from that of the hinged blades. The hinged blades have phase-angle response equal to or close to 90 degrees. However, the flapping deformation of the cantilever blade lags the force input by only 60 to 70 degrees. It should be noted that the cantilever blade phase lag is far from that of a truly rigid rotor which would have a phase lag of zero degrees. Due to the difference in phase-angle response the control phasing must be retarded from the conventional 90 degrees

to the order of 60 degrees. This "retardation," indicated on figure 2, must be incorporated into the cantilever rotor control system in order to eliminate large, undesirable cross-coupling in rotor response to lateral and longitudinal control inputs.

Another area where the reduced phase-angle response of the hingeless rotor requires attention is in regard to rotor pitch and roll angular-velocity damping. Here again, the force inputs to the blade associated with rotor angular velocity in pitch and roll originate from once-per-rotor-revolution gyroscopic and aerodynamic sources. The result is that the basic hingeless-rotor angular-velocity response is also cross coupled in the lateral and longitudinal directions. In other words, a longitudinal (pitching) angular velocity produces a lateral rotor moment as well as the direct longitudinal rotor damping moment.

Analytical Methods

In order to treat the control and damping response of the hingeless-rotor system in a relatively simplified manner and to utilize conventional rotor analysis, the cantilever blade can be replaced by an equivalent offset hinge blade, which is considered as a rigid body, with spring restraint at the hinge as shown in figure 3. The equivalence is derived and described in reference 2. The equivalent offset blade is established on the basis of the cantilever blade mode shape, nonrotating natural frequency, and rotating natural frequency. The equivalent offset is established to give the approximate bending-mode shape and Southwell coefficient, or frequency rise factor, of the cantilever blade. The equivalent offset in nondimensional form is given by

$$\epsilon_V = \frac{e_V}{R} = \frac{K_{1F} - 1}{2K_{1F} - 1} \tag{7}$$

In order to provide complete dynamic equivalence some hinge spring restraint is required and the spring constant is such as to give a nonrotating hinged-blade natural frequency ω_{1S} equal to that of the nonrotating cantilever blade. The spring constant is given by

$$K_{VF} = I_V \omega_{1S}^2 \tag{8}$$

This spring restraint at the hinge will be representative of the level of cantilever structural stiffness. For a typical case the contribution of this structural stiffness to the total rotating blade stiffness is about 5 percent of the total. In other words, the centrifugal force field still provides the major portion of flapwise stiffening, even for the cantilever system. Therefore, for the flapwise degree of freedom, the cantilever blade deformations and the influence of centrifugal force on the deformed blade are essentially the same as for a conventional offset hinge blade. However, it is necessary to include the hinge spring in the equivalent blade treatment so that the

cantilever blade mode shape, flapping angles, natural frequencies, blade response phase angles, and root bending moments can be simulated properly.

With the equivalent offset and spring restraint established on the basis of the cantilever blade first-mode characteristics, the cantilever blade root moments and effective flapping angles can be calculated using conventional hinged-rotor analysis. The first harmonic blade root moments and phase angles calculated using the equivalent offset blade and spring restraint will be equal to the first harmonic cantilever blade root moments and phase angles. This equivalence is also derived in reference 2.

In general, the cantilever blade flapping response will result in effective blade flapping angles β_1 which are very nearly equal to those of conventional offset hinged blades. In contrast to the similarity in the amplitude of blade motion, a most significant difference between the hinged and cantilever blade is the magnitude of the moments transmitted to the rotor shaft. The effective offset and spring restraint of the cantilever blade serve to develop large moments at the rotor hub. The magnitude of these moments are of an order-of-magnitude greater than those normally associated with hinged-rotor systems.

Rotor Moment Characteristics

The control-moment and angular-velocity damping-moment characteristics of a hingeless-rotor system can be calculated using the concept of an equivalent hinged blade with an 8- to 12-percent offset and with spring restraint at the hinge. The conventional offset hinged-blade flapping equations can be used with suitable modifications to account for the hinge spring restraint.

The results of sample calculations are shown in figures 4 and 5 for an equivalent offset value of 10 percent. The longitudinal and lateral hub moments, in nondimensional form, are presented for a range of blade Lock number and blade nonrotating first-mode natural-frequency ratio, ω_{1S}/Ω. Current cantilever blade designs have a nonrotating flapwise frequency ratio of ω_{1S}/Ω on the order of 0.2.

Figure 4 indicates that the direct longitudinal moment per degree of lateral blade cyclic feathering input is accompanied by lateral, or cross coupled, moment. For a given value of ω_{1S}/Ω the amount of cross coupling varies with blade Lock number γ due to the affect of aerodynamic damping on phase response. This indicates that there will be variations in control-moment response associated with large changes in altitude. Figure 5 presents direct and cross-coupled rotor pitching-velocity damping-moment trends. Here again, the moment response is cross coupled and strongly influenced by blade Lock number for any given value of ω_{1S}/Ω. This indicates there will be altitude effects on the angular-velocity damping-moment response of the rotor.

While the solution to control-moment cross coupling lies in some form of control input "retardation," the solution to cross-coupled angular-velocity

damping may require careful selection of blade stiffness and Lock number or the use of some feedback system which is sensitive to aircraft angular velocity. The rotor control-moment and damping-moment capability indicated in figures 4 and 5, even for blades with low values of ω_{1S}/Ω, are an order-of-magnitude greater than conventional helicopter rotor capability. This increased moment capability was demonstrated during the wind-tunnel tests of a full-scale hingeless-rotor helicopter at the NASA-Ames Research Center. The results of this investigation are presented in reference 3. This increased moment capability suggests that careful attention must be given to the blade root and rotor hub structural loads.

FLIGHT INVESTIGATION

In order to proceed with an exploratory flight investigation with a hingeless-rotor system, NASA purchased from Bell Helicopter Company a duplicate of an existing set of experimental hingeless-rotor components. The configuration was identical to that of the rigid hub rotor described in reference 4. The test aircraft is shown in figure 6.

Test Aircraft, Instrumentation and Procedure

The basic aircraft was an Army H-13G helicopter. The standard teetering rotor and the control linkage above the swashplate were removed and replaced by the experimental three-bladed hingeless-rotor system. The rotor blades were modified H-13H metal blades. The modification consisted of removal of a section of blade tip and adding a 12-pound tip weight. The resulting rotor radius was 190 inches with the modified blade mounted on an experimental rotor hub, as shown in figure 7. The hub was intentionally overdesigned so as to provide generous margins of safety.

The principal feature of the main rotor blade pitch control linkage arrangement was the phasing used between the control inputs at the swashplate and the feathering axis of the rotor blades. This phasing was reduced from the usual 90 degrees to 62.5 degrees and corresponds to a control "retardation" of 27.5 degrees. This "retardation" was discussed in general in the first section of this paper, in connection with cantilever blade response, and was illustrated in figure 2. No artificial stabilization devices were used during the investigation and the horizontal stabilizer, normally used on the H-13 aircraft, was removed prior to beginning the test program.

Since the principal innovation in the hingeless-rotor-system concept is the capability to transfer large moments from the rotor system into the hub and rotor shaft, attention was focused on the measurement of the structural bending moments in this area. The blade root, hub, rotor shaft, and control linkages were the primary components selected for strain-gage instrumentation. Flight-test instrumentation was also installed for the measurement of the necessary parameters to document the aircraft's flying qualities. These parameters included aircraft angular velocities and control positions.

The test program consisted of 14 hours of operation. During the program, data were obtained for various ground and flight operating conditions. In general, the flight conditions investigated included level flight throughout the forward speed range, autorotation, vertical descents, steep turns in level and autorotative flight, abrupt maneuvers, and slope take-offs and landings.

Control Characteristics

While the documentation and analysis of the aircraft flying qualities are treated in references 5 and 6, a brief mention of the aircraft's control characteristics is included here in order to illustrate the influence of rotor dynamics on the flying-qualities evaluation. The response of the hingeless-rotor system was very rapid when compared to the response of the typical articulated-rotor system as illustrated in the right-hand portion of figure 8. Because of the tight response, the pilot received early and clear evidence of the angular velocity developed by a given control input. The measured control power and damping values are an order-of-magnitude greater than conventional articulated rotors. This comparison is presented in the right-hand portion of figure 8. This increase in control power and damping is also reflected in the calculated values for the H-13 hingeless rotor also shown in figure 8. This calculated control power and damping was obtained using the equivalent-offset flapping blade approach discussed in the first portion of this paper. The new level of control and response capability led, ultimately, to the performance of more abrupt and more severe maneuvers, hence, directly influencing the structural loads experienced.

While the overall level of control power and damping improved significantly, the presence of cross coupling in the pitch and roll response was noted by the pilot and was borne out by the measured response to purely longitudinal- and lateral-control step inputs. The measured response to a longitudinal-control step input and to a lateral-control step input is shown in figure 9. This figure is in the form of plots of aircraft pitching angular velocity versus rolling angular velocity resulting from unit step inputs in the longitudinal direction and in the lateral direction. The curves may be viewed as representations of variation in magnitude and direction of the resultant aircraft angular velocity following the control step inputs. As previously mentioned, the installed control retardation was 27.5 degrees. Also shown on the figure, for comparison purposes, are the calculated response curves based on the results of the equivalent-offset blade analysis and the coupled pitch and roll equations of motion for the aircraft.

The most significant points to be noted here are (1) the difference in the phasing between initial angular-velocity response and final steady-state angular-velocity direction and (2) the dropoff in the final measured roll angular-velocity response. The shift in response phase was due to cross coupling during the maneuvers and the shift was particularly objectionable to the pilot, especially in the roll maneuvers. The large reduction in the final roll angular velocity indicated by the measured data in figure 9, is attributed to a strong dihedral effect, which was not included in the calculated curves. The calculated response curves, including 27.5 degrees control retardation, compare

reasonably well with the measured results. The calculated curves, without control retardation included, indicate that very undesirable response characteristics would be expected. The results of this investigation suggest the need for careful attention during the detailed design of a hingeless-rotor system so as to minimize the effects of cross coupling. This will involve careful selection of blade stiffness, Lock number, control retardation and the possible use of an angular-velocity feedback system.

Structural Loads

The objective of the structural loads portion of this investigation was to sample all the practical ground and flight operating conditions in an effort to identify those conditions which require most immediate and detailed study. The rotor system possessed control capability of sufficiently large magnitude to cause concern over the large-amplitude cyclic loadings that could be induced in the primary structure of the aircraft. The following discussion treats some of the more significant results of the structural loads investigation.

Ground operation.- The ground-operation investigation was limited to observing the trends in the rotor-blade and rotor-shaft bending moments. Due to the fact that the rotor shaft was designed for use with a teetering rotor system, the allowable cyclic bending-moment amplitude was established at 1500 foot-pounds on the basis of rotor-shaft fatigue test data. Inasmuch as the hingeless-rotor system had the capability of producing hub moments on the order of 1200 foot-pounds per degree of cyclic control input, extreme care had to be exercised by the pilot to keep the cyclic stick centered during ground run-up and lift-off. It was necessary for the pilot to anticipate the cyclic trim position during transition from the ground to the airborne condition in order to avoid large transients in rotor-shaft cyclic bending moment.

Structural loads trends were observed during slope take-offs and landings. It was determined that the best control technique to minimize cyclic bending moments in the rotor system was to apply almost full collective control prior to bringing the aircraft to a level attitude with cyclic control. The reverse control sequence was used in slope landings. In addition to pilot technique, there are a number of available approaches toward the reduction of the rotor shaft bending moments, such as reducing gear tread width, but it will require specific design attention.

Flight loads.- The in-flight structural loads encountered are considered in two categories - first, those measured in level flight and, second, the loads measured in maneuver flight.

Level flight: The level-flight structural loads in primary rotor components are summarized in figure 10. Although the test rotor was fabricated from standard articulated components (except for the hub itself), the measured loads experienced in level flight throughout the speed range were not above the design "fatigue limit" for these components. "Fatigue limit" is defined as the cyclic load amplitude which results in a fatigue life equal to 10^8 cycles.

· Maneuver flight: During the test program, structural loads were monitored carefully as the flight envelope was expanded in order to assure safety of flight. In general, the high loadings were not of a critical nature, and the increase in load level with severity of the maneuver was certainly not unexpected, especially with regard to rotor shaft and blade flapwise bending moments. The structural loading of most concern was the "in-plane," or chordwise bending moments induced in the rotor blades. The amplitude of the rotor blade chordwise cyclic bending moment was very sensitive to maneuvers in which high aircraft angular velocities were developed. In some instances the amplitude of this loading expanded well beyond the structural fatigue limit, during pitch and roll maneuvers that were well within the control capability of the aircraft.

The buildup of cyclic chordwise blade bending moment with aircraft angular velocity occurred in pitch and roll maneuvers throughout the forward speed range. This is illustrated in figures 11 and 12, where sample time histories of the blade and mast bending moments are presented for a hovering maneuver and a maneuver at a forward speed of 70 knots. The relative magnitudes of the chordwise, flapwise, and mast bending moments are not presented to scale in these figures. The sample loads measurements presented in figure 11 are for the hovering maneuver where the pilot executed a longitudinal control step displacement and recovery. During the period of maximum pitching angular velocity, the buildup of the cyclic chordwise bending moment reaches a maximum amplitude which is above the structural fatigue limit of the blade. The oscillatory flapwise bending moments increased in amplitude during the recovery maneuver, but do not show the degree of sensitivity to the maneuver exhibited by the chordwise bending moment. The mast moments during the initial portion of the maneuver do not build up due to the application of a control moment because the initial control moment cancels a moment due to minor center-of-gravity offset. However, during the recovery, where the control moment and the offset center-of-gravity moment add, the cyclic mast moments reach a maximum during maximum angular acceleration.

The situation at a forward speed of 70 knots is shown in figure 12. Again the chordwise bending moment shows the large buildup with aircraft angular velocity and again above the structural fatigue limit. Continuous operation at this load level would result in a 10-hour fatigue life for this rotor blade. In contrast to the loads measured in hovering and the 70-knot maneuver conditions are the loads measured during a maneuver performed in autorotation. In this situation there was a complete lack of chordwise cyclic bending-moment buildup, even though an angular velocity of 0.4 rad/sec was obtained. This autorotation case involved low blade coning and reduced blade flapwise cyclic bending moments.

From the standpoint of structural loads, the sensitivity of the blade cyclic chordwise bending-moment amplitude to maneuvers was the primary concern in the flight investigation. Therefore, the principal goal of the analytical work of this investigation was to establish the relationship between rapid aircraft maneuvers and the high-amplitude chordwise bending moments.

ANALYSIS OF MANEUVER LOADS

A theoretical analysis of the oscillatory chordwise bending moments during maneuver conditions was performed using an extension of the equivalent offset hinged-blade analysis. In this case the equivalent offset and hinge spring restraint were determined for the lagging degree of freedom and the moment equation about the virtual lag hinge was derived for the maneuvering conditions. As a result of an assumption of identical first bending mode shapes for the flapwise and lagging degree of freedom the effective lag hinge offset is identical to the flapping hinge offset and the lag hinge spring constant is:

$$K_{VL} = I_v \nu_{1S} \tag{9}$$

The results of this analysis indicate that, for a given configuration, the blade oscillatory chordwise bending moment buildup during maneuvers is primarily dependent upon the amplitude and phase relation between blade flapping deformation β_1 and blade cyclic feathering motion θ_1 as follows:

$$M_{VL} = -K_{VL}\Gamma_L\gamma_v\left[C_3\beta_1 \cos\left(\psi - \Phi_{\beta,1} + \frac{\pi}{2}\right) + C_5\theta_1 \cos\left(\psi - \Phi_{\theta,1}\right)\right] \tag{10}$$

where

$$C_3 = -\left(\frac{\theta_o}{8} + \frac{\theta_t}{10} - \frac{2M_w\eta}{\gamma_v I_v \Omega^2}\right) \tag{11}$$

$$C_5 = \frac{1}{6}\left(C_T/2\right)^{1/2} \tag{12}$$

$$\Gamma_L = \left[1 - \frac{3}{2}k_1\epsilon_v - \left(\frac{\nu_{1S}}{\Omega}\right)^2\right]^{-1} \tag{13}$$

$$k_1 = \frac{2}{3}\frac{\sigma_v R}{I_v} \tag{14}$$

An example of how the flapping deformations and feathering motions combine to give large-amplitude chordwise bending moments is illustrated in figure 13. This figure is a polar plot of the recovery portion of the pitch maneuver in hover shown in figure 11. The polar plot shows the β_1, θ_1, $M_{C,1}$ situation at the time of maximum nose-down pitching angular velocity or approximately the 19th revolution in figure 11. The β_1, θ_1, and $M_{C,1}$ values presented in figure 13 have been nondimensionalized by dividing by their respective maximum values during the maneuver, and the resulting values are indicated by the

symbols in the figure. The blade flapwise bending moments, and therefore the flapwise deformations β_1, are occurring in the azimuth region of 270 degrees. These lateral flapping deformations result in maximum flapping velocities in the vicinity of zero degrees azimuth. These flapping velocities, in turn, induce blade cyclic chordwise moments primarily as a result of Coriolis effects. The maximum blade feathering motion θ_1 required to perform the recovery maneuver occurs at an azimuth of approximately 320 degrees.

The calculated values of blade chordwise moment, also in a nondimensional form, are shown in figure 13 by the heavy dashed lines. The direct aerodynamic induced chordwise moment is in-phase with the feathering motion and the Coriolis induced chordwise moment is in-phase with the flapping velocity, which is 90 degrees ahead of the flapping deformation. The resultant calculated chordwise moment, also shown in figure 13, compares reasonably well with the measured maximum chordwise moment amplitude and phase angle.

A detailed comparison of calculated and measured chordwise bending-moment amplitude and phase-angle time histories was performed for the hovering maneuver and the 70-knot maneuver case of figure 12. The difference between the maximum measured and calculated chordwise moment amplitude was approximately 15 percent of the maximum measured amplitude. The agreement obtained in these comparisons indicates that the equivalent offset method is adequate for first-order estimates of the more significant structural loading problems of the hingeless-rotor system. Examination of the autorotation case indicated that the theory would predict low-cyclic chordwise moments in the maneuver, which is in agreement with the measured results.

As noted in equation (10), the amplitude of the blade chordwise bending moment is proportional to blade chordwise structural stiffness K_{VL}, and this offers a means of alleviating the chord load sensitivity to maneuvers by reducing the blade chordwise stiffness.

DYNAMIC MODEL INVESTIGATION

As part of the hingeless-rotor research program, Langley has taken part in a cooperative effort involving U.S. Army, Lockheed Aircraft, and NASA. This program has involved the design, construction, and wind-tunnel testing of a 1/3-scale hingeless-rotor helicopter model, which was aeroelastically scaled. The model rotor was 10 feet in diameter. The program proceeded in three phases. The first-phase testing was done in Langley 30-foot by 60-foot full-scale tunnel and the second- and third-phase testing was done in the Langley 16-foot transonic dynamics tunnel. The results and analysis of the testing are published in references 7 and 8.

A considerable number of dynamic configurations were tested during the program. Research information of general interest resulting from the program included structural load and aerodynamic data for the various rotor configurations. Rotors tested included those with twisted and untwisted blades; three-,

four-, and six-blade rotors; and variations in blade flapwise and chordwise stiffness and stiffness distribution. Each of these configurations was tested through a forward-speed and load-factor g range simulating conventional helicopter and compound helicopter operation.

Structural Loads

Seven rotor configurations were tested in the Langley 30-foot by 60-foot full-scale tunnel. These tests covered a simulated speed range from hovering to 120 miles per hour and load factors up to 2.5g. A photograph of the model installation in the tunnel test section is shown in figure 14. The rotor configurations tested were all 3-bladed and the blades were of wide chord giving a rotor solidity of 0.12. The testing in the full-scale tunnel was done to study a variety of rotor dynamic configurations at low and moderate forward speeds prior to testing selected configurations at high forward speeds in the transonic dynamics tunnel. The model was dynamically scaled in all respects except Mach number and Reynolds number for the initial testing.

Some of the highlights of the structural loads results from the full-scale tunnel testing are shown in figures 15, 16, and 17. In part (a) of each figure curves are shown for three rotor configurations in 1g trimmed flight conditions. One configuration represents conventional blade design with a blade cantilevered from the rotor hub which had a very high chordwise stiffness relative to its flapwise stiffness. The second configuration was the same blade with a reduced chordwise stiffness at the root achieved by using a flexible drag link. The stiffness of the drag link was such that the static deflection of the blade tip under a tip load was equal in both the flapwise and chordwise direction. The third configuration was such that along the entire blade the chordwise structural stiffness was approximately equal to the flapwise blade stiffness.

The variation in oscillatory blade torsional load throughout the speed range is shown in figure 15(a). The corresponding variation in the magnitude of cyclic flapwise bending moment is shown in figure 16(a). There were no significant influences of chordwise blade stiffness or stiffness distribution in the case of the torsional and flapwise moments. From the standpoint of structural loads, the most significant result of the testing is shown in figure 17(a) which shows the amplitude of cyclic chordwise moment at the blade root for 1g flight over the simulated speed range. As indicated in the figure, there is a large increase in chordwise cyclic load with increasing speed for the conventional blade (that is, for a blade with high chordwise stiffness and low flapwise stiffness). By using a flexible drag link at the blade root to reduce the blade chordwise stiffness to match the flapwise stiffness a large reduction in chordwise cyclic loading was obtained over the entire speed range. An even greater reduction in the loads was achieved by matching the chordwise stiffness to the flapwise stiffness along the entire blade.

While the results presented in part (a) of figures 15, 16, and 17 are for 1g flight, the effects of variations in load factor were investigated and the results are presented in part (b) of figures 15, 16, and 17. As indicated in figure 17(b), large reductions in blade chordwise cyclic bending moments were again obtained with the introduction of chordwise flexibility.

The introduction of blade flexibility as a means of reducing chordwise structural loading may offer the solution to the problem of high cyclic chordwise moments experienced in the flight-test maneuvers mentioned in the first part of this paper (figs. 11 and 12). As indicated in equation (10) and demonstrated in the wind-tunnel-test results the blade chordwise stiffness K_{VL} is a primary factor in determining the magnitude of the chordwise cyclic loading. Therefore, a reduction in blade chordwise stiffness will result in a reduction in blade structural bending moments. Care must be taken to achieve this stiffness reduction, without substantial reduction in chordwise section modulus, especially in the rotor hub region, so that the net result is a decrease in blade stress levels. This can be handled by proper selection of materials, cross-section configuration, and stiffness distribution along the blade. The benefits of increased chordwise flexibility will apply to both steady flight conditions and to maneuver conditions since the key to the reduced structural moments is the centrifugal relieving moments developed on a flexible blade.

Additional Wind-Tunnel Tests

Following completion of the model tests in the full-scale tunnel at scaled forward speeds up to 120 mph, the model was tested in the Langley 16-foot transonic dynamics tunnel. In these tests the model was reballasted and tested in Freon at a density of 0.008 slug-per cubic foot and dynamic and aerodynamic scaling was achieved including Mach number and Reynolds number similitude. The model is shown installed in the transonic dynamics tunnel in figure 18. The basic configuration tested was the 3-blade rotor with matched root flapwise and chordwise blade stiffness. Aerodynamic and structural load data were obtained with simulated forward speeds from 60 to 240 mph and tip Mach number up to 0.91. Conventional helicopter and compound helicopter modes of operation were sampled and the results are presented in reference 7.

Additional tests were made using a blade and rotor hub design optimized for low drag. The blades were of more conventional aspect ratio and the blade flapwise and chordwise stiffness were approximately matched along the entire blade. Rotors with 3, 4, and 6 blades were tested with rotor solidities of 0.06, 0.08, and 0.12, respectively. The 3-blade model configuration is shown in figure 19. As in previous tests, structural loads and performance data were obtained for a range of load factors and forward speeds in the helicopter and unloaded rotor mode of operation. The following listing represents the maximum operating conditions reached with the unloaded rotor configurations.

V_{sim}	$\frac{\Omega}{\Omega_n}$	M_{tip}	μ
258	1.0	0.95	0.58
272	.85	.88	.72
266	.71	.79	.85

The data obtained in the final phase of testing are presented in reference 8. The "optimized" rotor design with the low chordwise stiffness blades shows considerable promise from the standpoint of structural loads, vibration and performance.

Ground Resonance

One of the areas which requires careful investigation in regard to the reduced chordwise stiffness blade design is the ground resonance phenomenon. Due to the fact that the blade "in-plane" first bending mode natural frequency falls below normal operating rotor speed, a coupling of the in-plane blade oscillation with body pitch or roll oscillation may occur during runup or shutdown of the rotor. This situation corresponds to the classical "ground resonance" experienced with hinged rotor systems. This coupling can also occur in flight with the hingeless-rotor system, due to the fact that the fuselage has a pitch and roll stiffness as a result of being spring mounted to the rotor through the cantilever action of the blades. This results in an "air resonance" phenomenon, which is equivalent to the classical ground resonance phenomenon.

An extensive theoretical analysis of the ground resonance phenomenon for the hingeless rotor has been carried out in reference 9. This analysis included rotor aerodynamics, and the results of this work, presented in reference 10, indicate that the coupled vibration mode can be stabilized without the addition of artifical damping. Basically, the studies reported in references 9 and 10, and other investigations reported in reference 11, indicate that the presence of the rotor aerodynamics tends to stabilize the coupled response of the rotor and fuselage. The stabilizing influence of aerodynamics results from the fact that the aerodynamically damped blade flapping degree of freedom is now coupled to body pitch and roll degree of freedom through the cantilever action of the blades. The analyses indicate that, if the aerodynamics is removed from the system, the dynamic response reverts back to the classical Coleman unstable ground resonance phenomenon.

During the third phase of model testing in the transonic dynamics tunnel, limited ground resonance type testing was conducted in air with the model ballasted for testing in Freon. This resulted in a dynamic simulation in which aerodynamic damping forces, relative to the mass and spring forces, were diminished by approximately 60 percent. Under these conditions, cases of unstable "ground resonance" were encountered. In order to assure safe operation in the tunnel the body pitch and roll frequencies were adjusted to eliminate resonance when operating in air at normal rotor speed. Operation still involved passing through a rotor speed at which body pitch natural frequency coincided with blade chordwise natural frequency in the nonrotating coordinate system. This situation is indicated in figure 20 at the intersection of the body pitch frequency curve and the $\left(\Omega - \nu_{1R}\right)$ curve. In the absence of aerodynamics this point theoretically corresponds to a condition of unstable ground resonance. Subsequent operation in Freon was carried out without experiencing unstable ground resonance.

A thorough study of the ground resonance problem was not undertaken during the tunnel program; however, this phenomenon will require further investigation in order to conclusively establish whether the reduced chordwise stiffness blade configurations can, in fact, be operated over a wide range of conditions without encountering mechanical instabilities of the ground resonance type.

CURRENT FLIGHT INVESTIGATION

As part of the continuing hingeless rotor program, an XH-51N helicopter, shown in figure 21, has been purchased by NASA. This aircraft is equipped with a 3-bladed hingeless rotor and represents an aircraft specifically designed to utilize the hingeless rotor system. The aircraft has been completely instrumented for handling qualities, performance, structural loads and dynamics investigations and is being used as a general research vehicle. The new capability of the hingeless rotor system will make it possible to investigate the influence of increased levels of control power and damping on the handling qualities criteria of reference 12.

A structural loads investigation will be conducted concurrently with the handling qualities program. The early portions of the structural loads program will deal with the general nature of the loads encountered in operation of the aircraft. Later, specific flight conditions will be flown to investigate structures and dynamics problems in detail.

CONCLUDING REMARKS

In general, the flight, wind-tunnel and analytical investigations carried out to date on the hingeless-rotor concept indicate there are definite improvements to be gained by proper application of the principle. It has been shown that the system cannot actually be treated as a "rigid" structure and, in fact, in the first flapwise mode it deforms much like a hinged system. The improvements associated with the hingeless rotor stem from its simplicity and the capability to develop large rotor hub moments. In actually utilizing the hingeless rotor design particular attention must be given to the problems of (1) control and damping cross coupling (2) structural loads in maneuvers, when using high chordwise blade stiffness and (3) the avoidance of ground resonance type instabilities, when using blades with low chordwise stiffness.

As a result of the research conducted to date, there appear to be promising avenues open to cope with the problems that have been identified; however, continuing research is required to explore these promising solutions. It will also be necessary to expand the analytical and experimental investigations in order to provide sufficient design criteria for the successful utilization of the hingeless-rotor system on advanced VTOL aircraft.

REFERENCES

1. Yntema, R. T.: Simplified Procedures and Charts for the Rapid Estimation of Bending Frequencies of Rotating Beams. NACA TN 3459, 1955.

2. Young, Dr. M. I.: A Simplified Theory of Hingeless Rotors With Application to Tandem Helicopters. American Helicopter Society Proceedings of the Eighteenth Annual National Forum, Washington, D.C., May 2-4, 1962, pp. 38-45.

3. McCloud, John L.; and Biggers, James C.: Full-Scale Wind-Tunnel Tests of Nonarticulated Helicopter Rotor. NASA TN D-2392, 1964.

4. Cresap, W. L.: Rigid Rotor Development and Flight Tests. Presented at the IAS 30th Annual Meeting, New York, New York, January 22-25, 1962.

5. Huston, Robert J.; and Tapscott, Robert J.: The Results of Some Wind Tunnel and Flight Studies With Helicopters at NASA. Presented at New York Academy of Sciences Conference on Vertical Take-Off and Landing Aircraft, New York, New York, December 10-12, 1962.

6. Ward, John F.; and Huston, Robert J.: A Summary of Hingeless-Rotor Research at NASA-Langley. Presented at the Twentieth Annual National Forum of the American Helicopter Society, Washington, D.C., May 13-15, 1964.

7. Hanson, T. F.: Investigation of Elastic Coupling Phenomena of High-Speed Rigid Rotor Systems. U.S. Army - TRECOM Technical Report 63-75. (Submitted under contract DA 44-177-TC-929 by Lockheed-California Company, March 1964.)

8. Hanson, T. F.: Wind Tunnel Tests of an Optimized, Matched-Stiffness Rigid Rotor. U.S. Army - TRECOM Technical Report 64-56. (Submitted under contract DA 44-177-AMC-78(T) by Lockheed-California Company, November 1964.)

9. Kanno, J. S.; and Lundgren, S.: Equations of Motion for the Dynamic Analysis of a Hovering Rotor Including Gyro Control System. Lockheed California Company, LR 17185, June 1961. (Submitted under U.S. Army - TRECOM contract DA 44-177-TC-828.)

10. Kanno, J. S.; and Lundgren, S.: 10-Foot Rigid Rotor Model Basic Data and Results of Hovering Cyclic Stability Analysis. LR 16997, July 1963. (Submitted under U.S. Army - TRECOM contract DA 44-177-TC-828.)

11. Reed, Wilmer H.: Propeller Whirl Flutter; A State-of-the-Art Review. Presented at the Symposium on the Noise and Loading Actions on Helicopter V/STOL Aircraft and Ground Effect Machines, University of Southampton, England, August 30 - September 3, 1965.

12. Anon.: Military Specification - General Requirements for Helicopter Flying and Ground Handling Qualities. MIL-H-8501A, 1961.

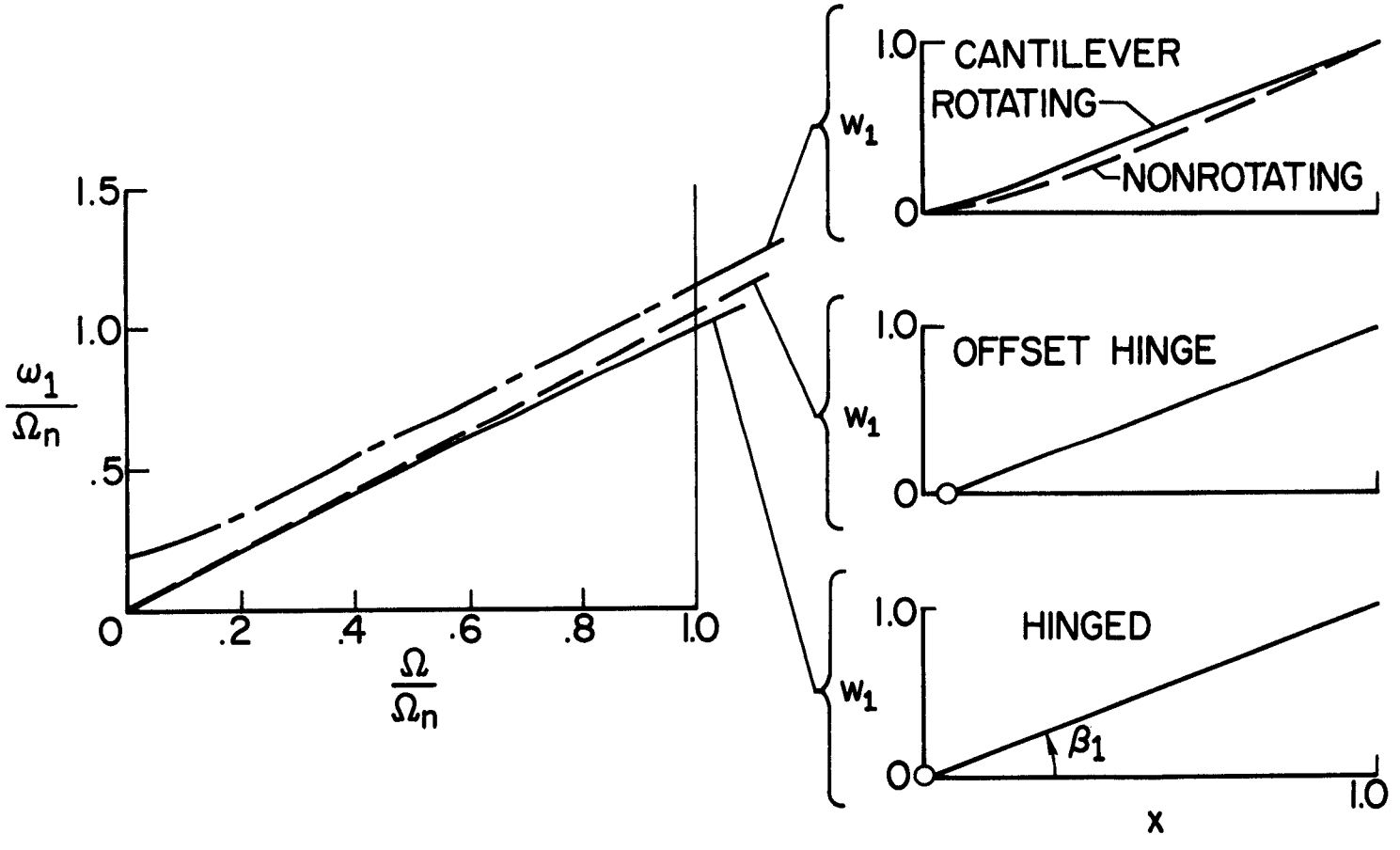

Figure 1.- Rotor blade natural frequencies and mode shapes.

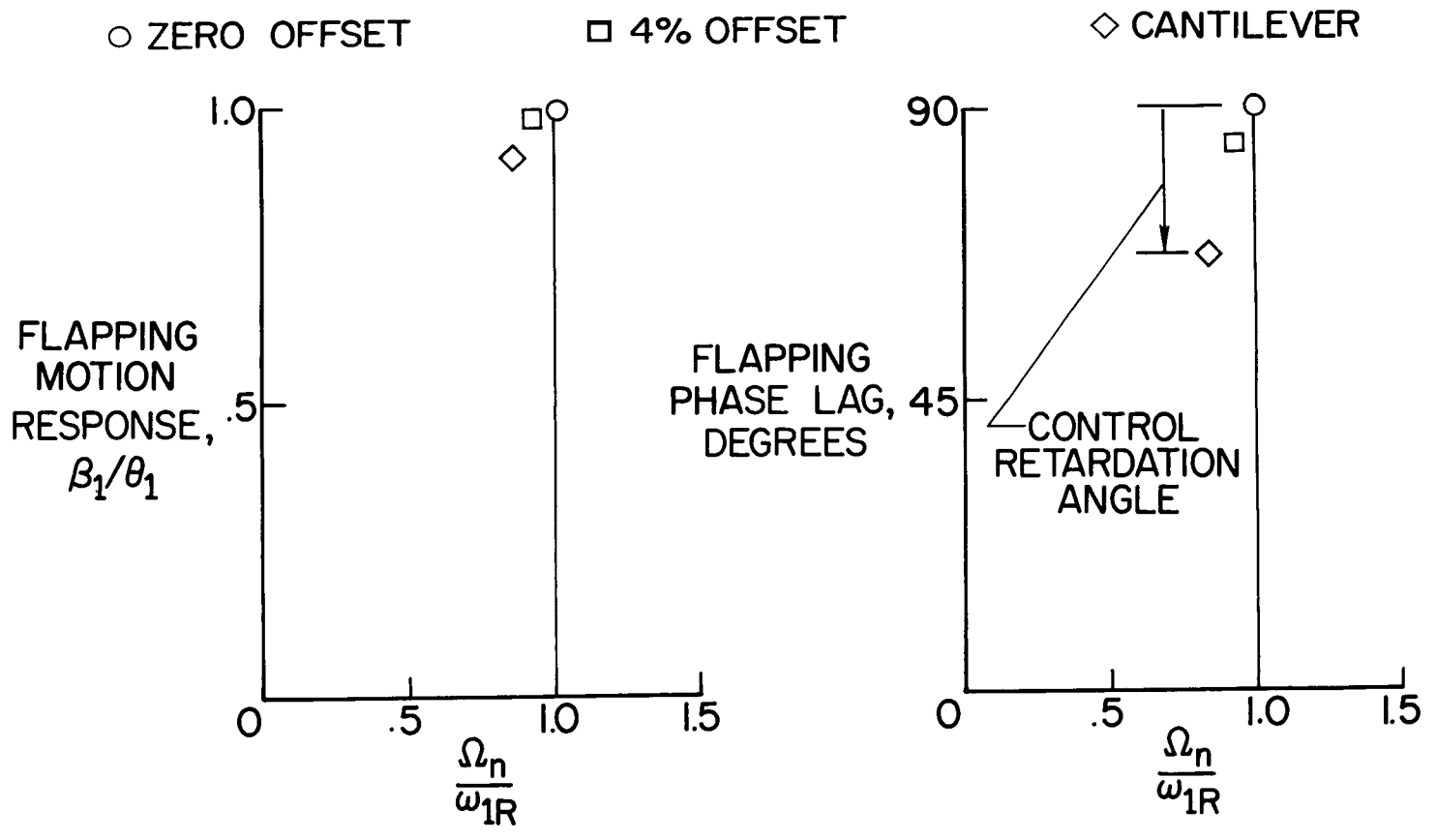

Figure 2.- Blade response to cyclic control input.

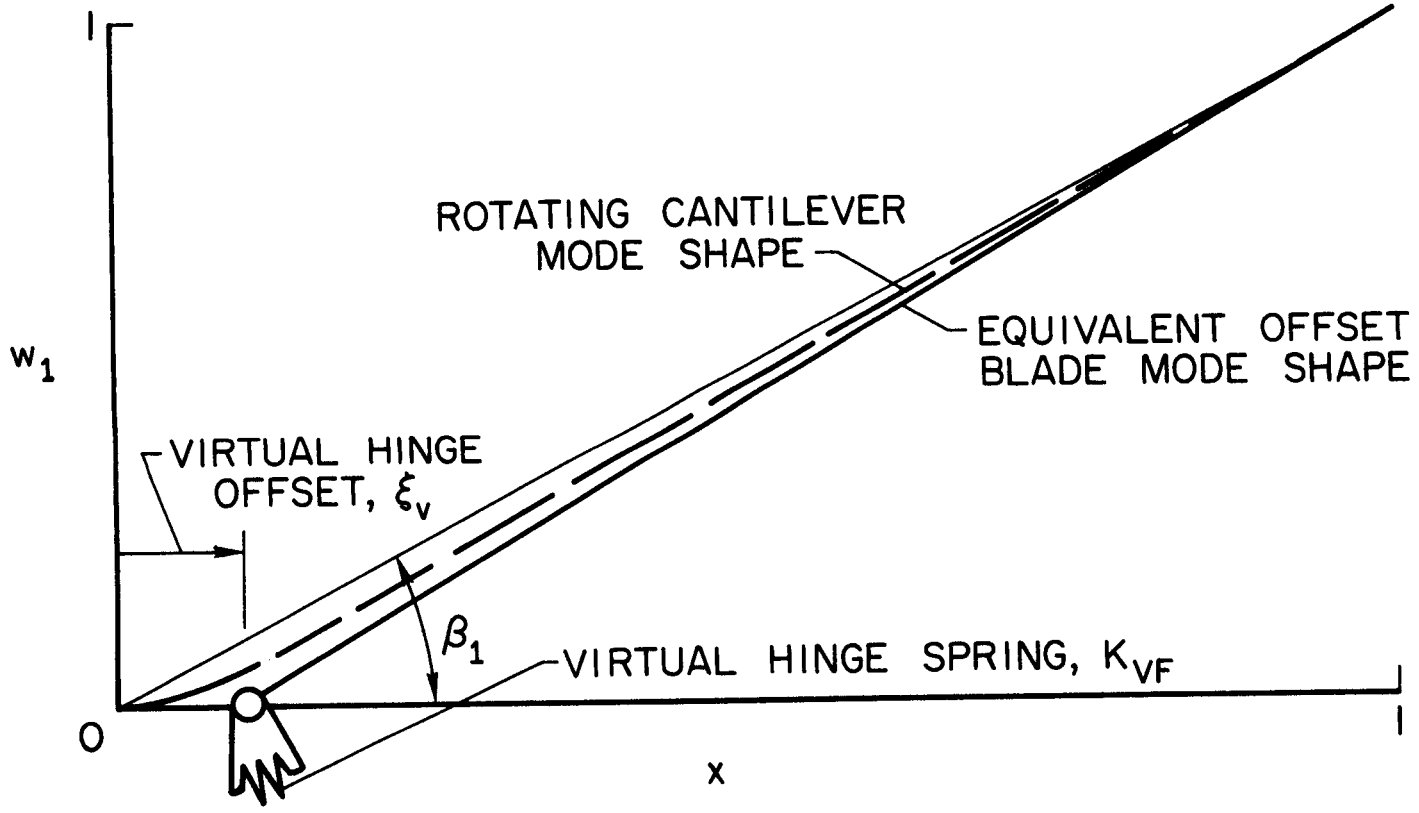

Figure 3.- Equivalent offset hinge blade with spring restraint.

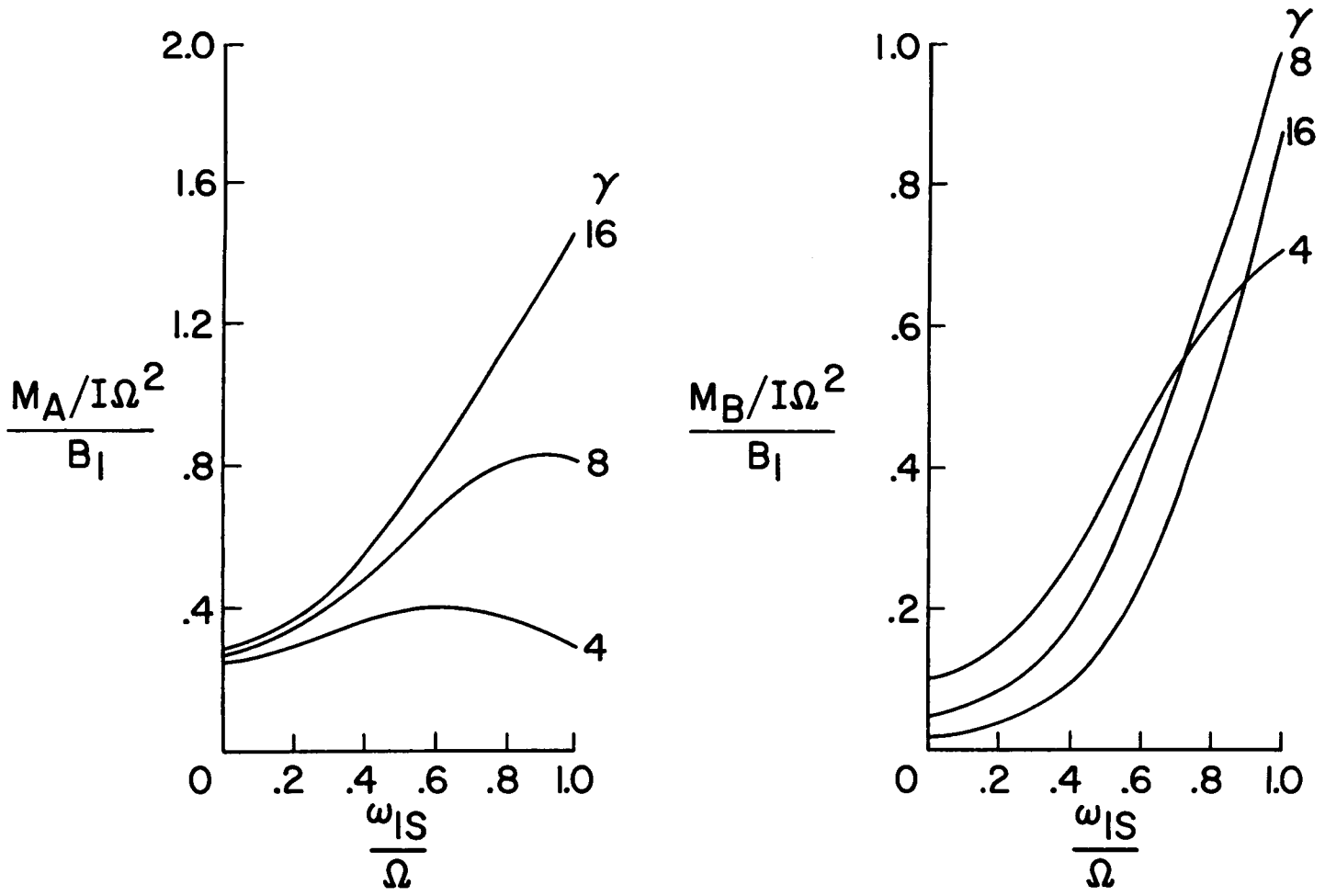

Figure 4.- Effect of blade stiffness and Lock number on rotor hub control moment and cross-coupling, $\xi_V = 0.10$.

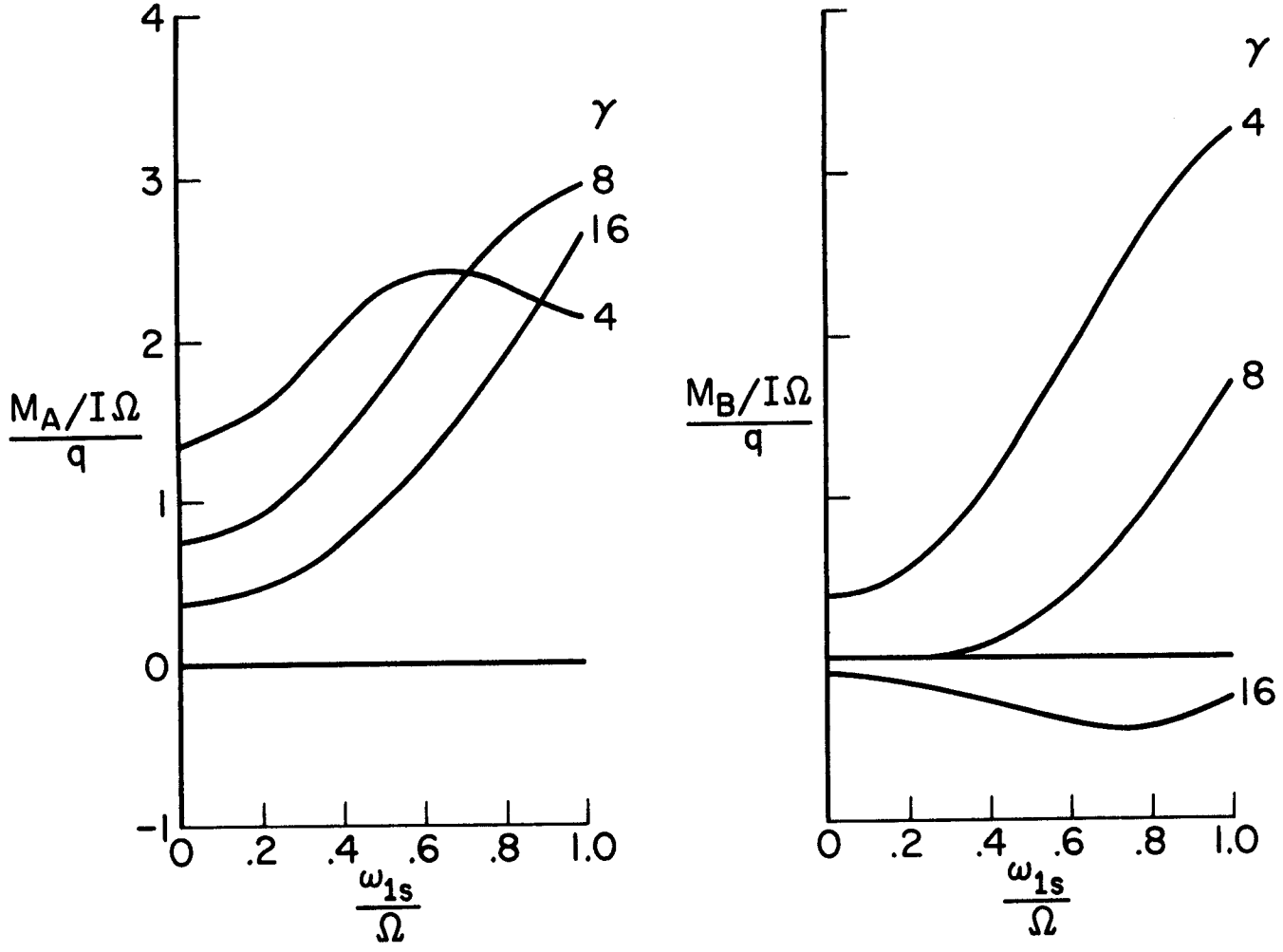

Figure 5.- Effect of blade stiffness and Lock number on rotor hub damping moment and cross-coupling, $\xi_v = 0.10$.

Figure 6.- Hingeless rotor on H-13G helicopter.

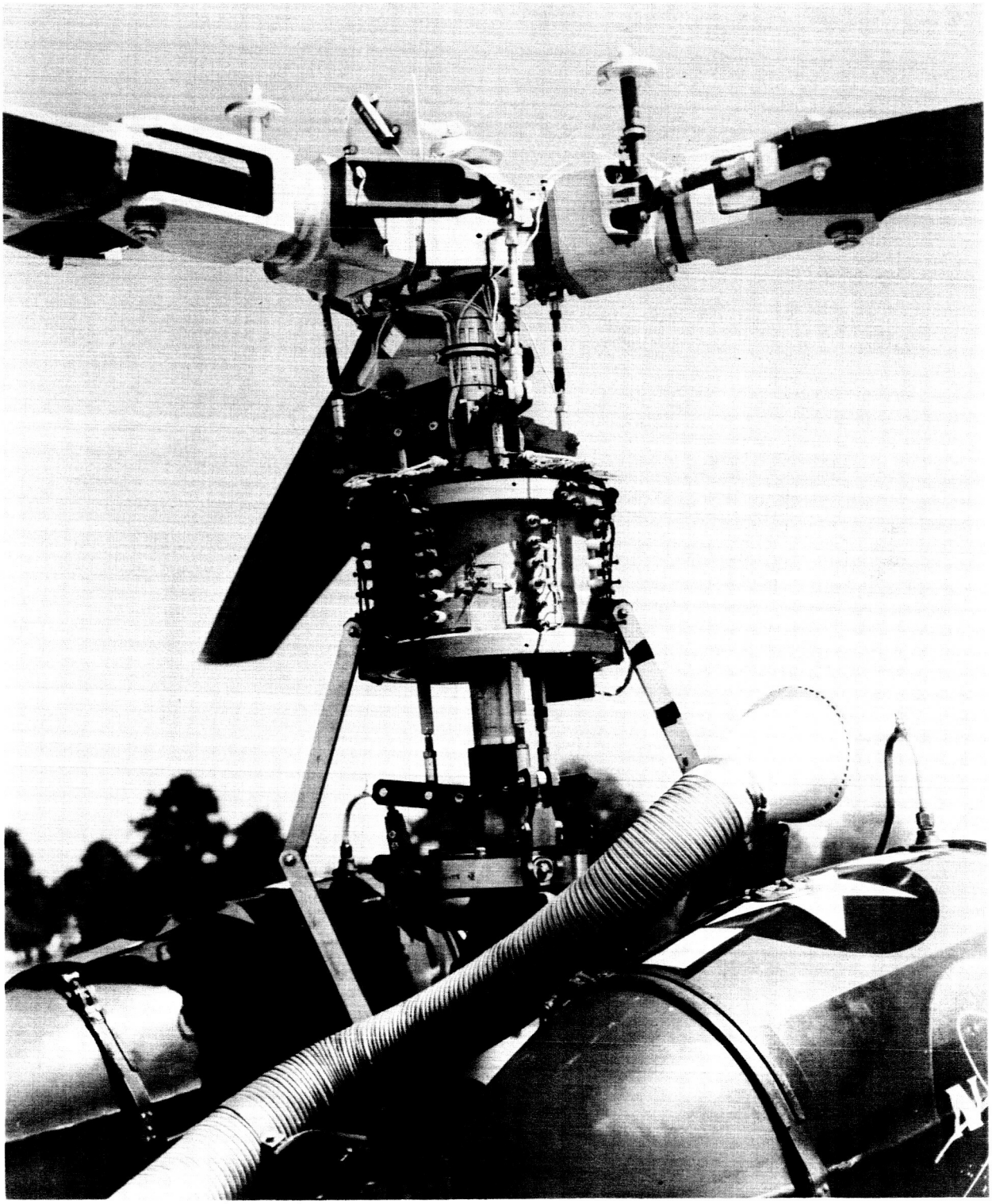

Figure 7.- Hingeless-rotor hub and slipring assembly.

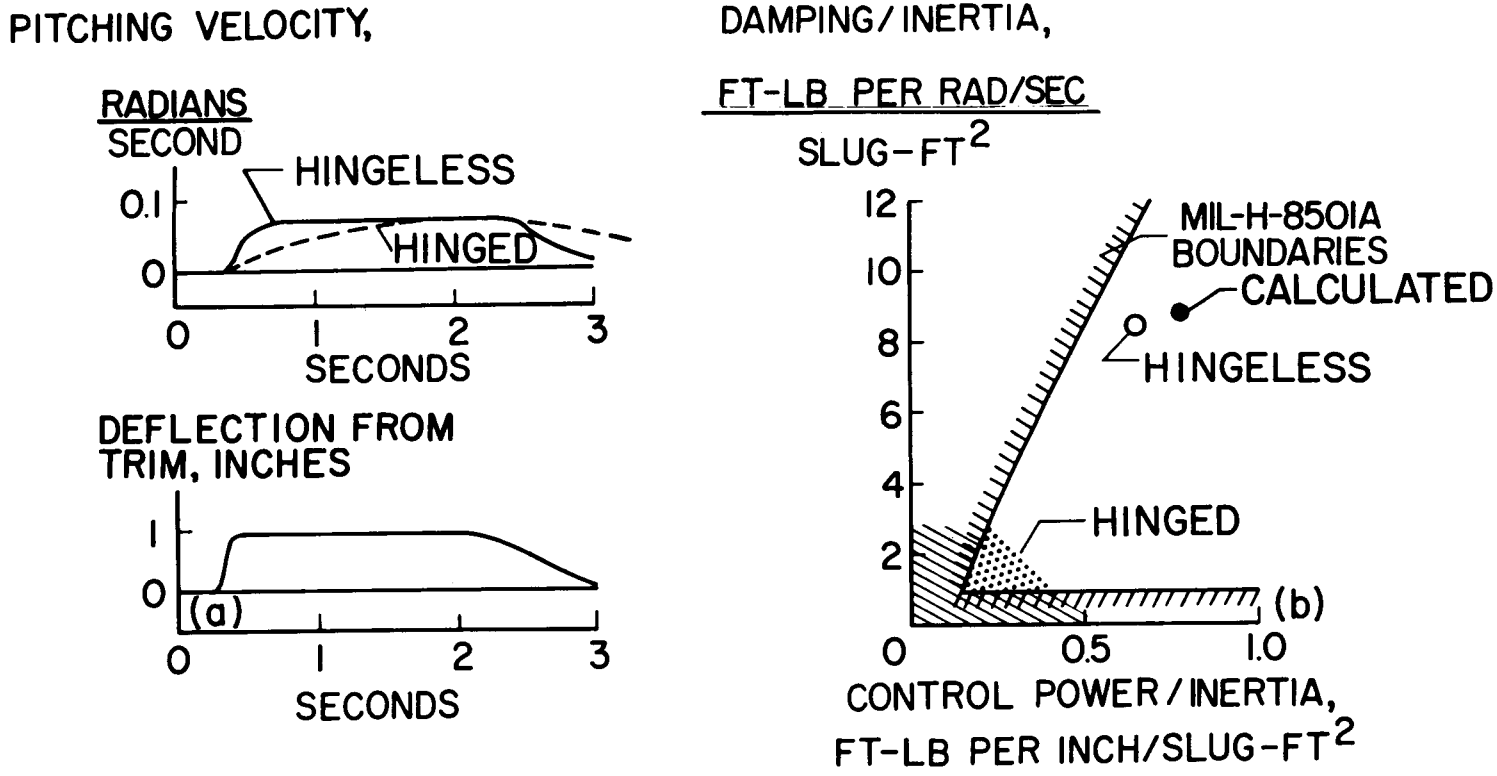

Figure 8.- Control-response and handling-qualities comparison of hingeless-rotor helicopter and conventional hinged-rotor helicopter in hovering flight.

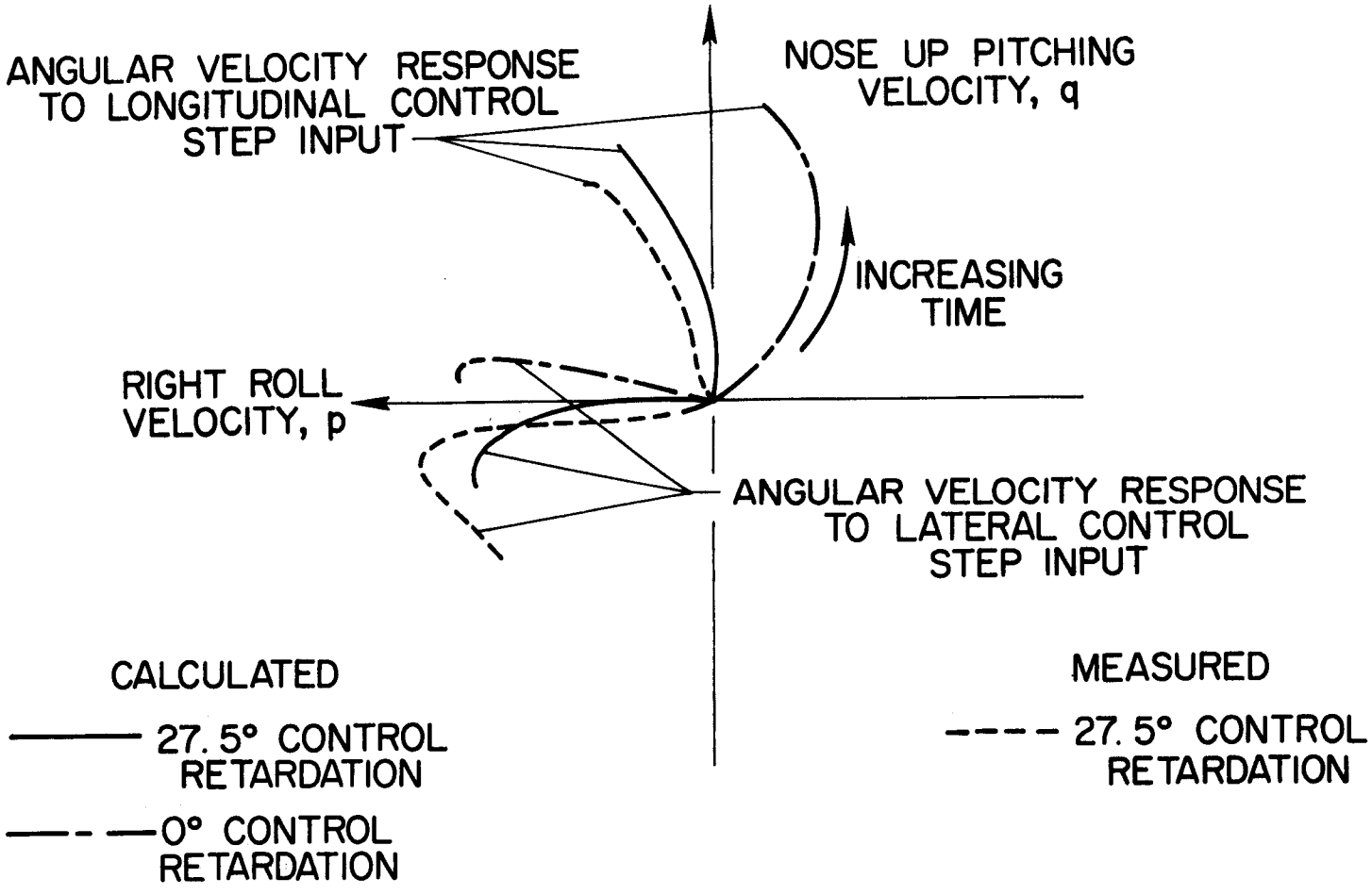

Figure 9.- Aircraft angular velocity response to lateral and longitudinal control step inputs.

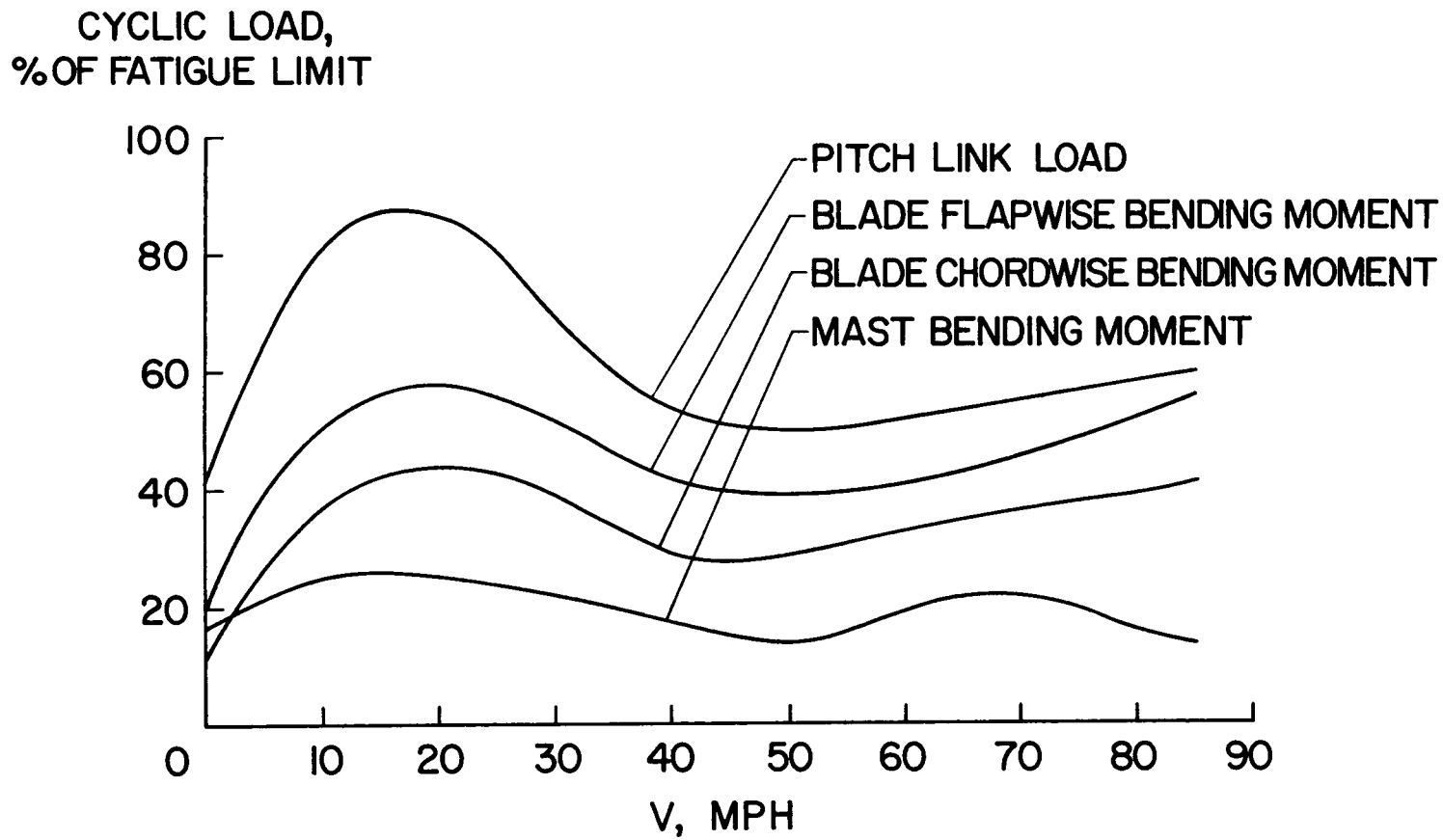

Figure 10.- H-13G hingeless-rotor cyclic structural loads in level flight.

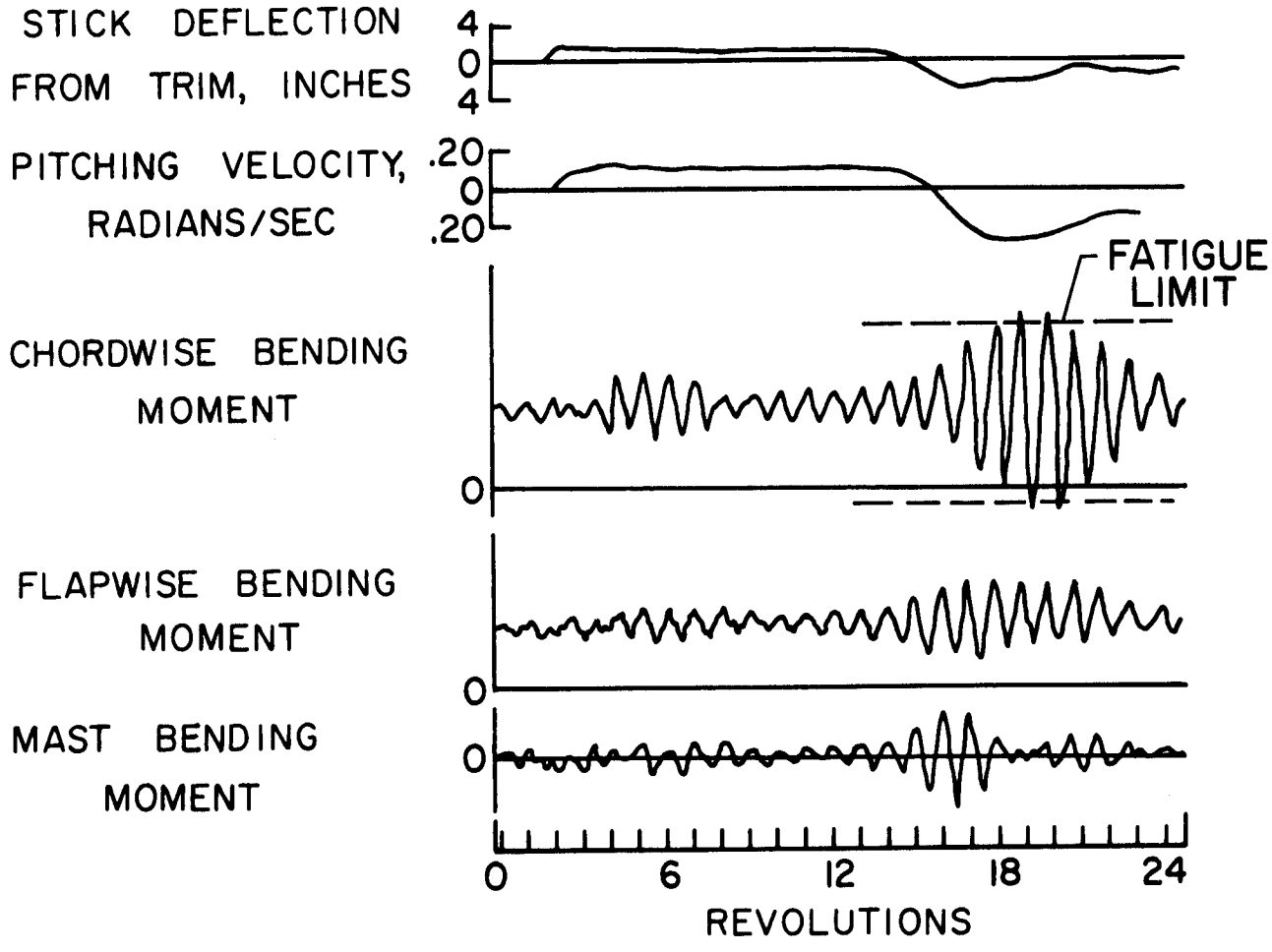

Figure 11.- Structural-loads time history during longitudinal maneuver and recovery with hingeless-rotor helicopter in hovering flight.

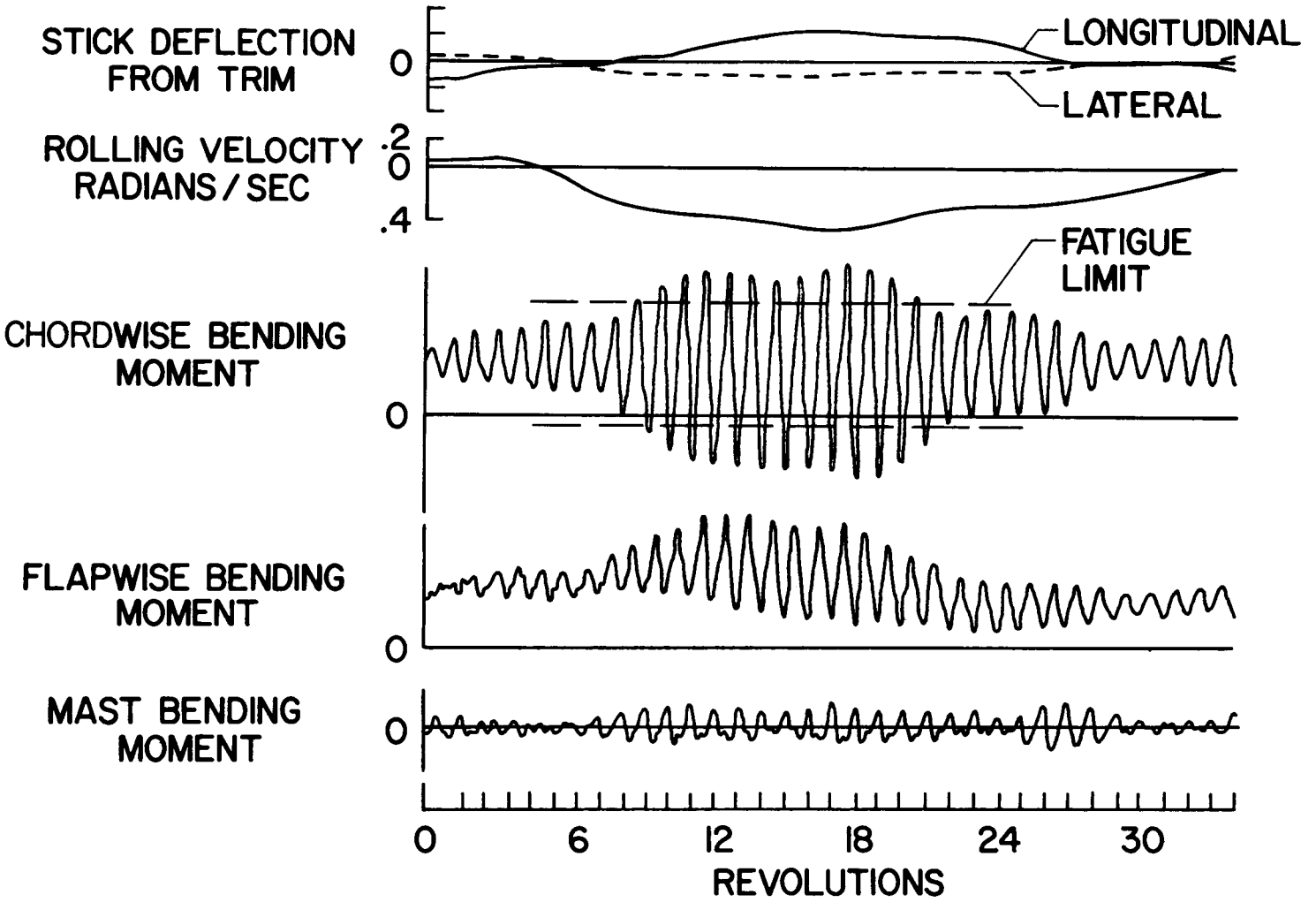

Figure 12.- Structural-loads time history during lateral maneuver with hingeless-rotor helicopter in level flight at a forward speed of 70 knots.

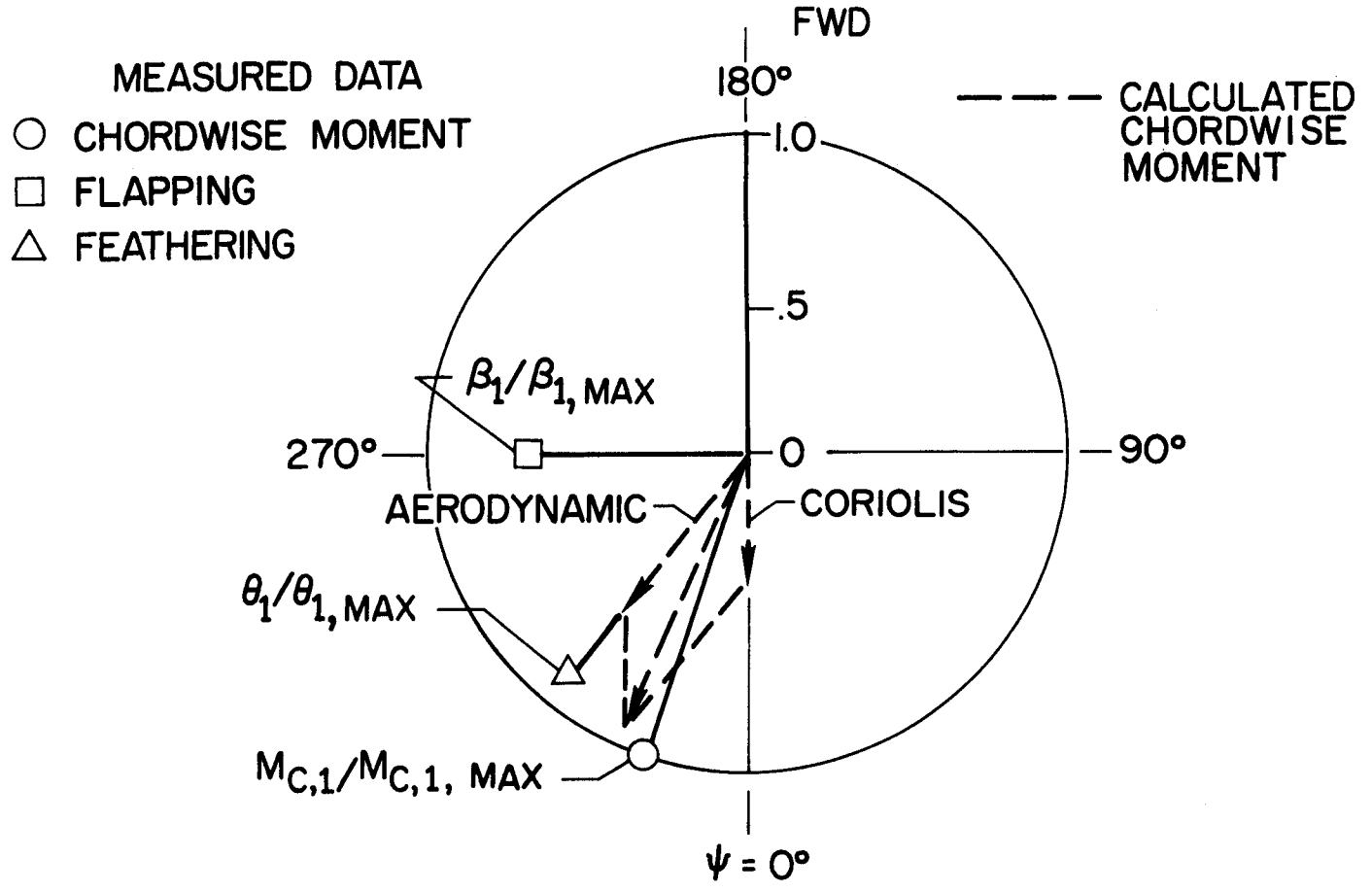

Figure 13.- Maximum blade cyclic chordwise bending moments in hovering pitching maneuver.

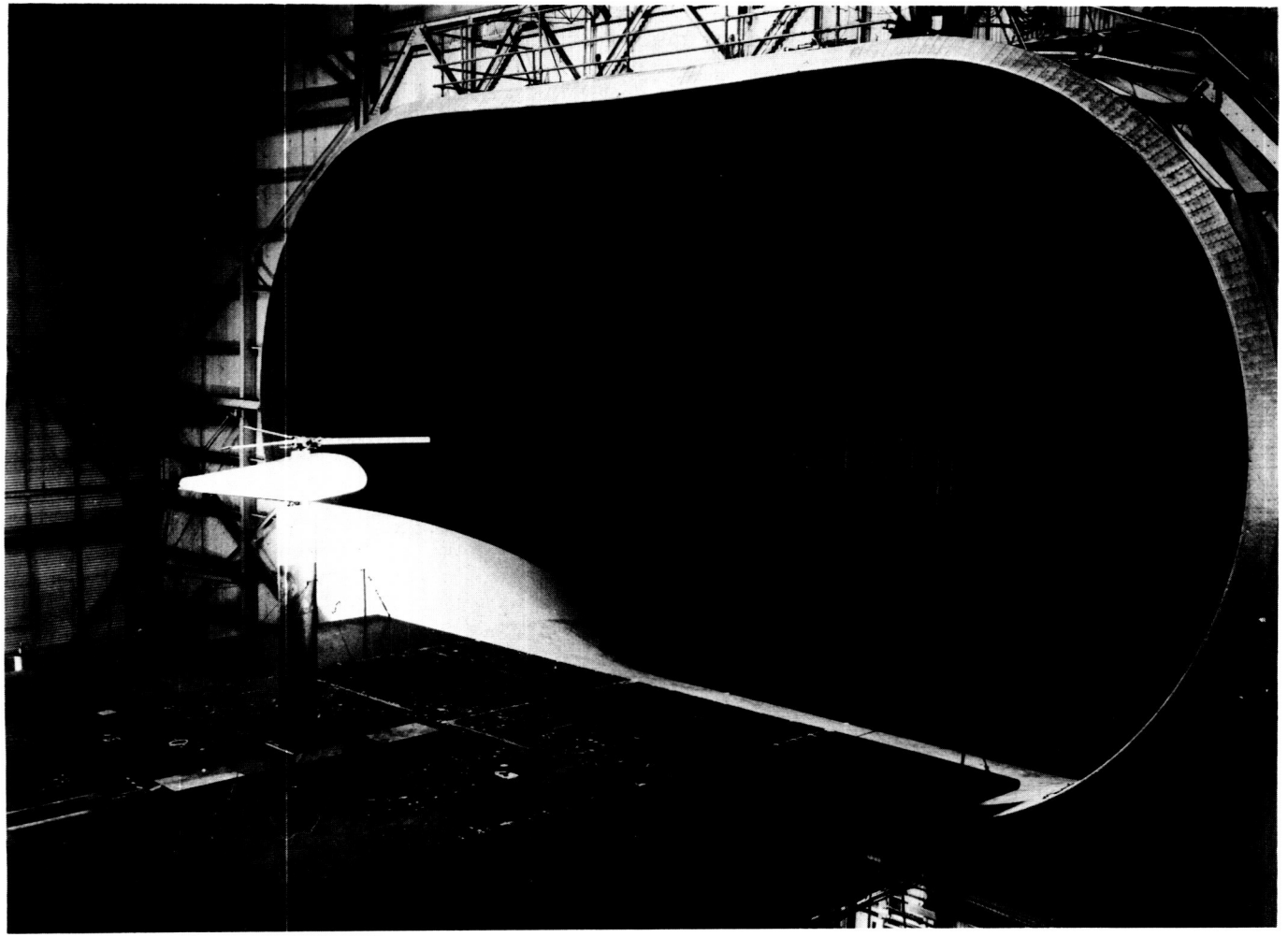

Figure 14.- Hingeless-rotor dynamic model in Langley 30-foot by 60-foot full-scale tunnel.

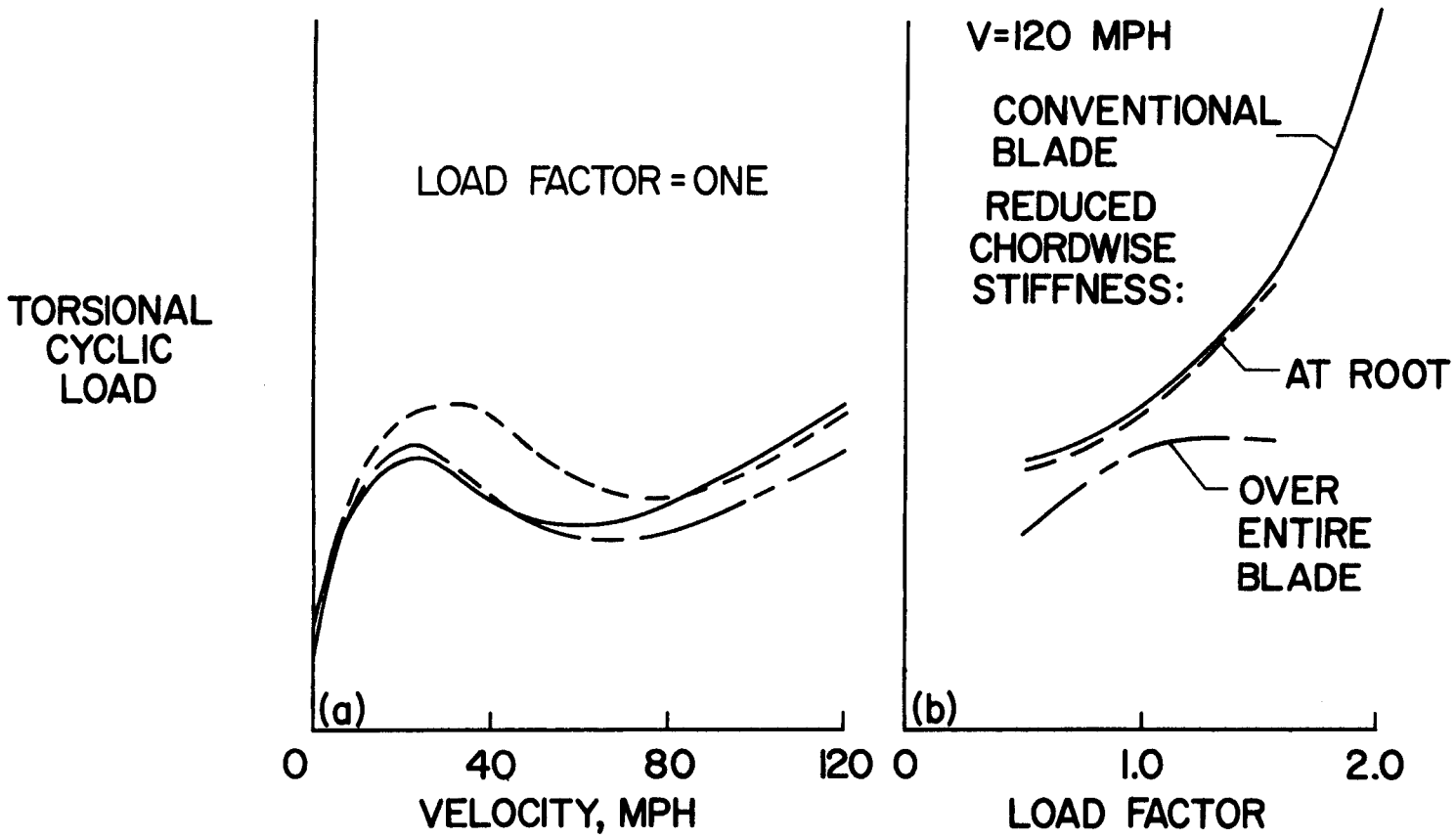

Figure 15.- Effect of blade chordwise stiffness on blade torsional cyclic load.

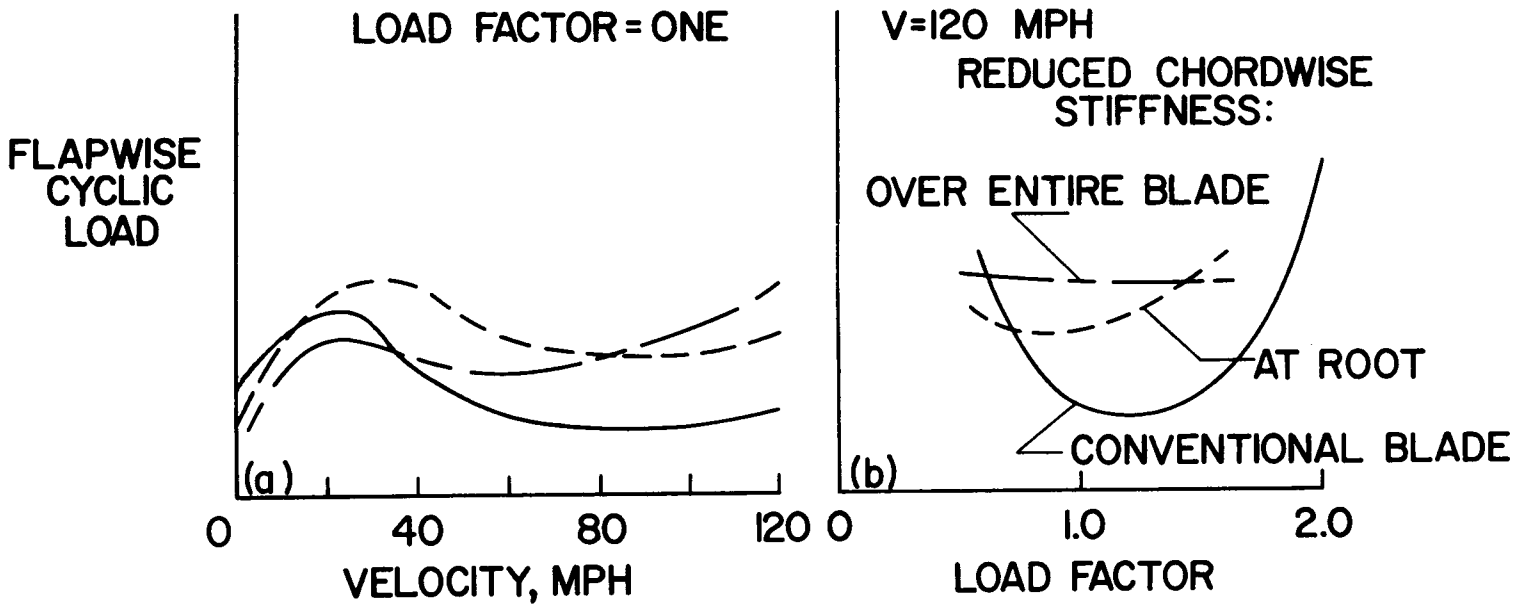

Figure 16.- Effect of blade chordwise stiffness on blade flapwise cyclic load.

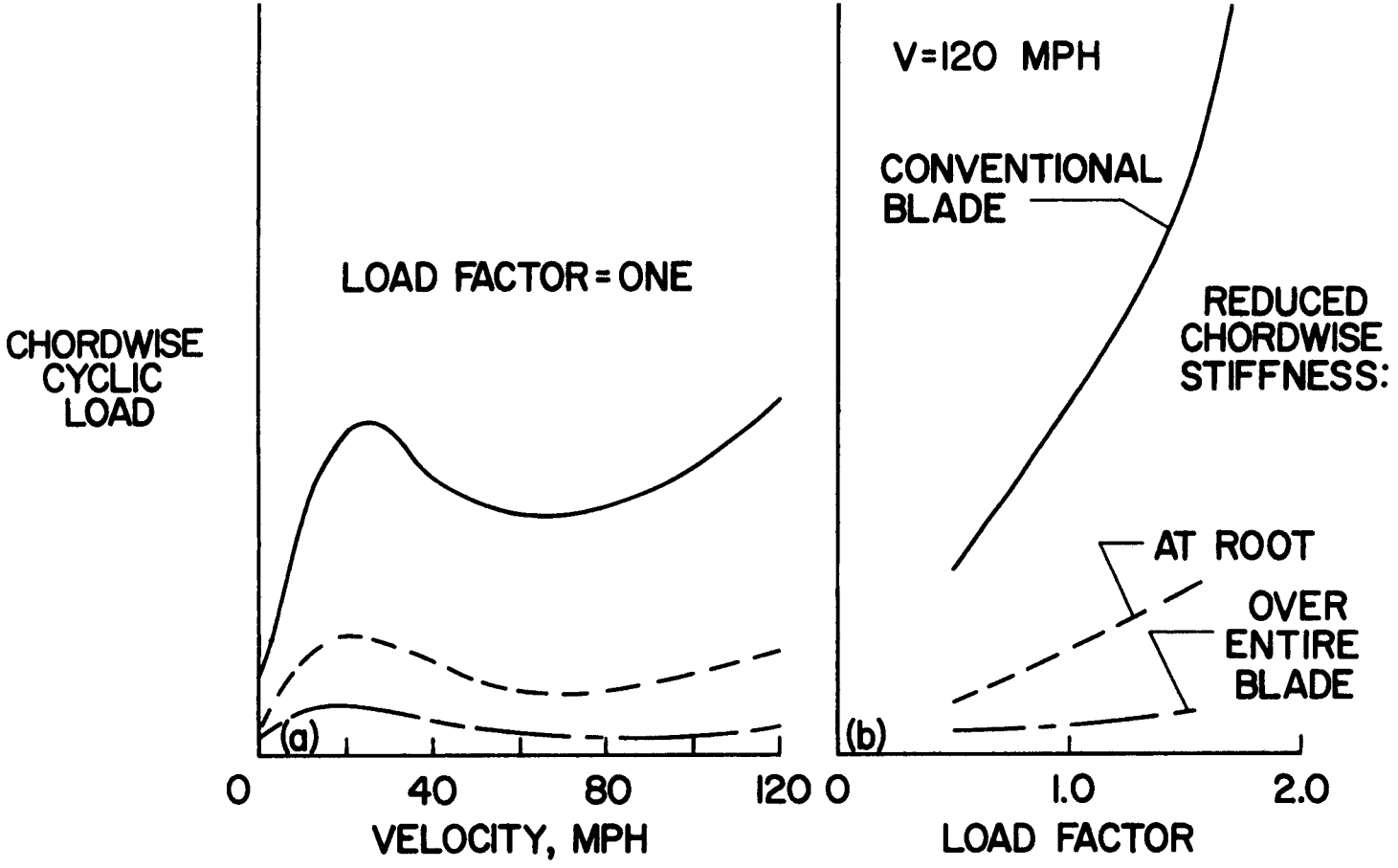

Figure 17.- Effect of blade chordwise stiffness on blade chordwise cyclic load.

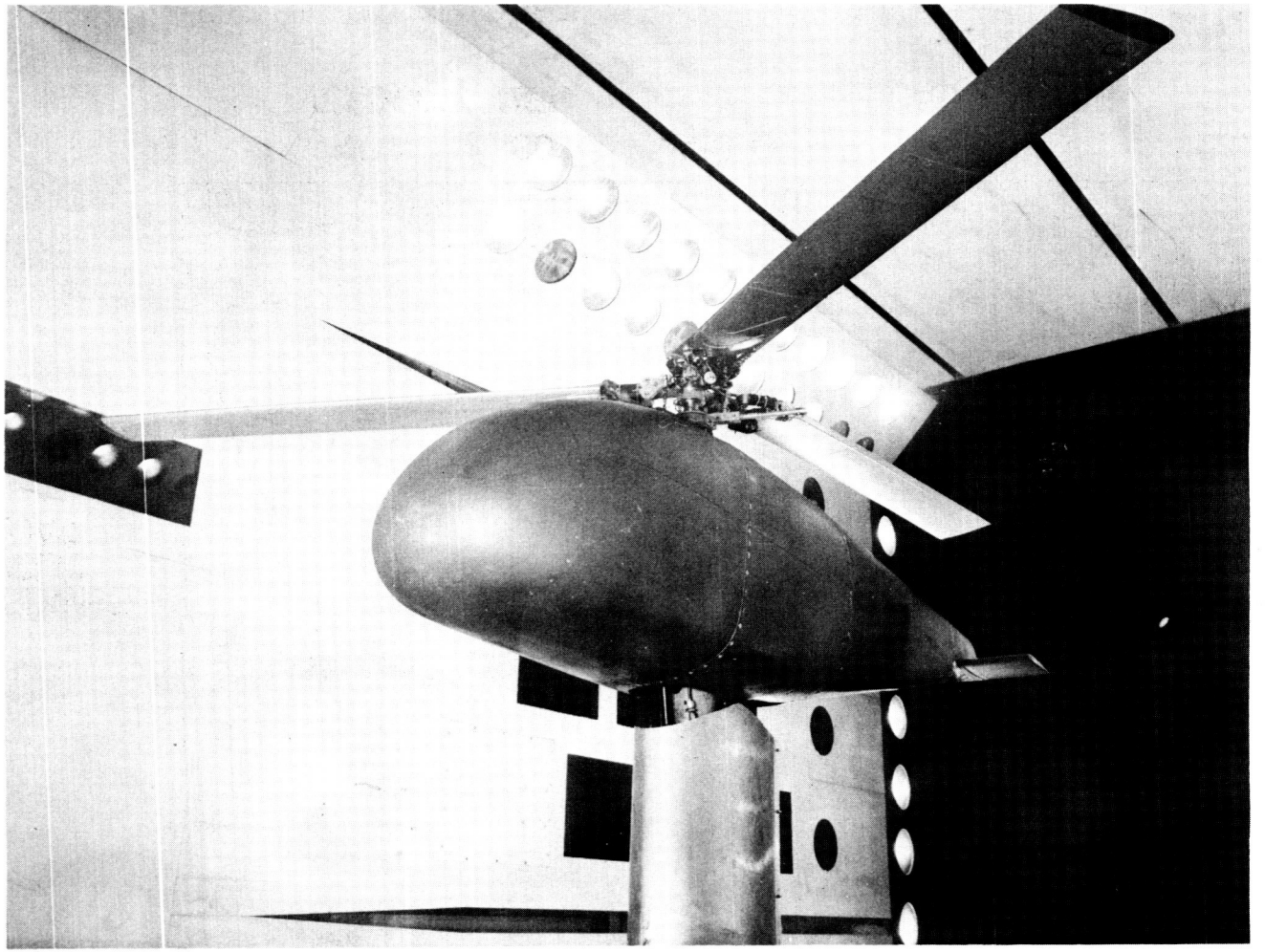

Figure 18.- Three-blade hingeless-rotor dynamic model in Langley 16-foot transonic dynamics tunnel (Solidity = 0.12).

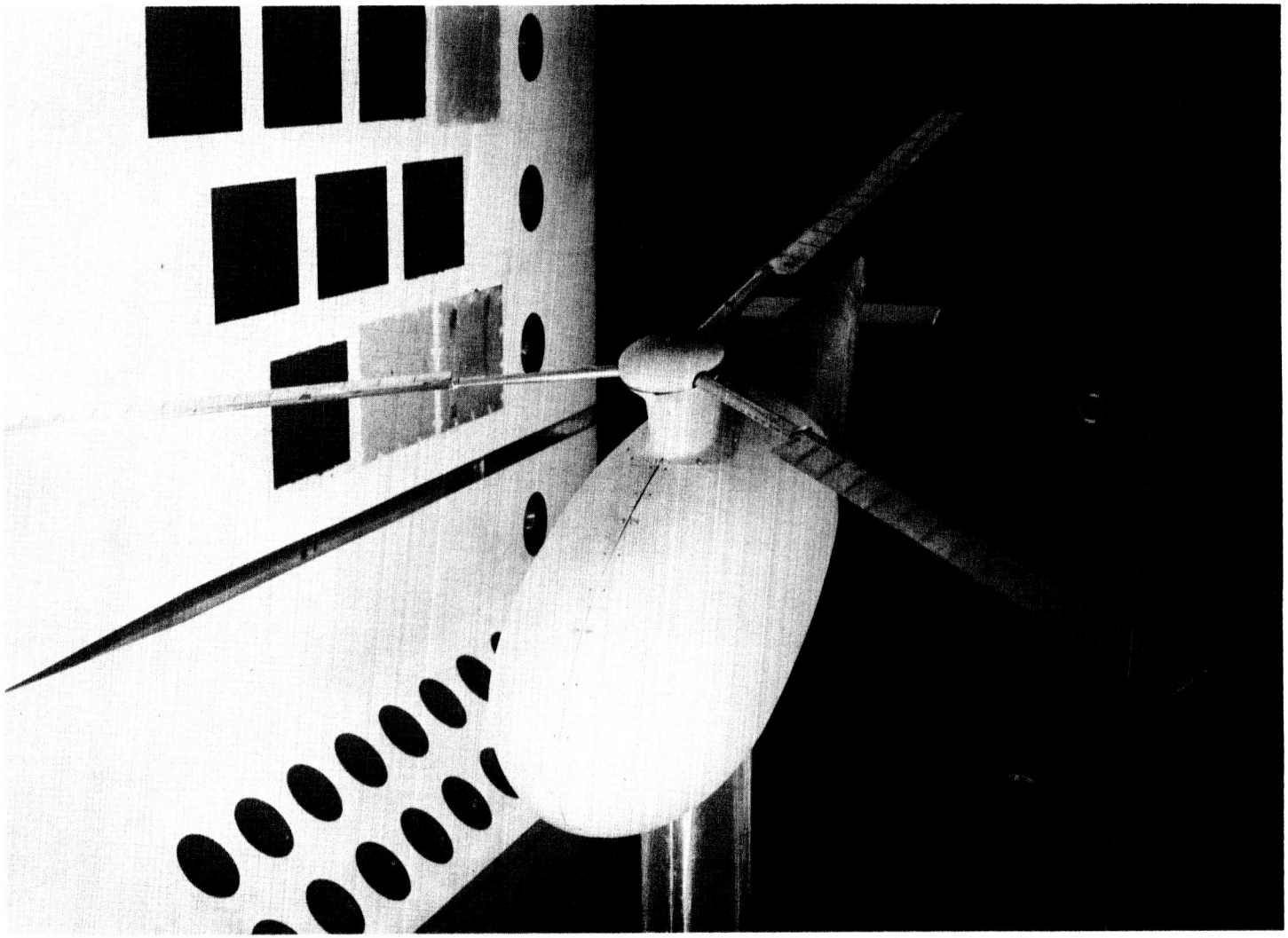

Figure 19.- Three-blade hingeless-rotor dynamic model in Langley 16-foot transonic dynamics tunnel (Solidity = 0.06).

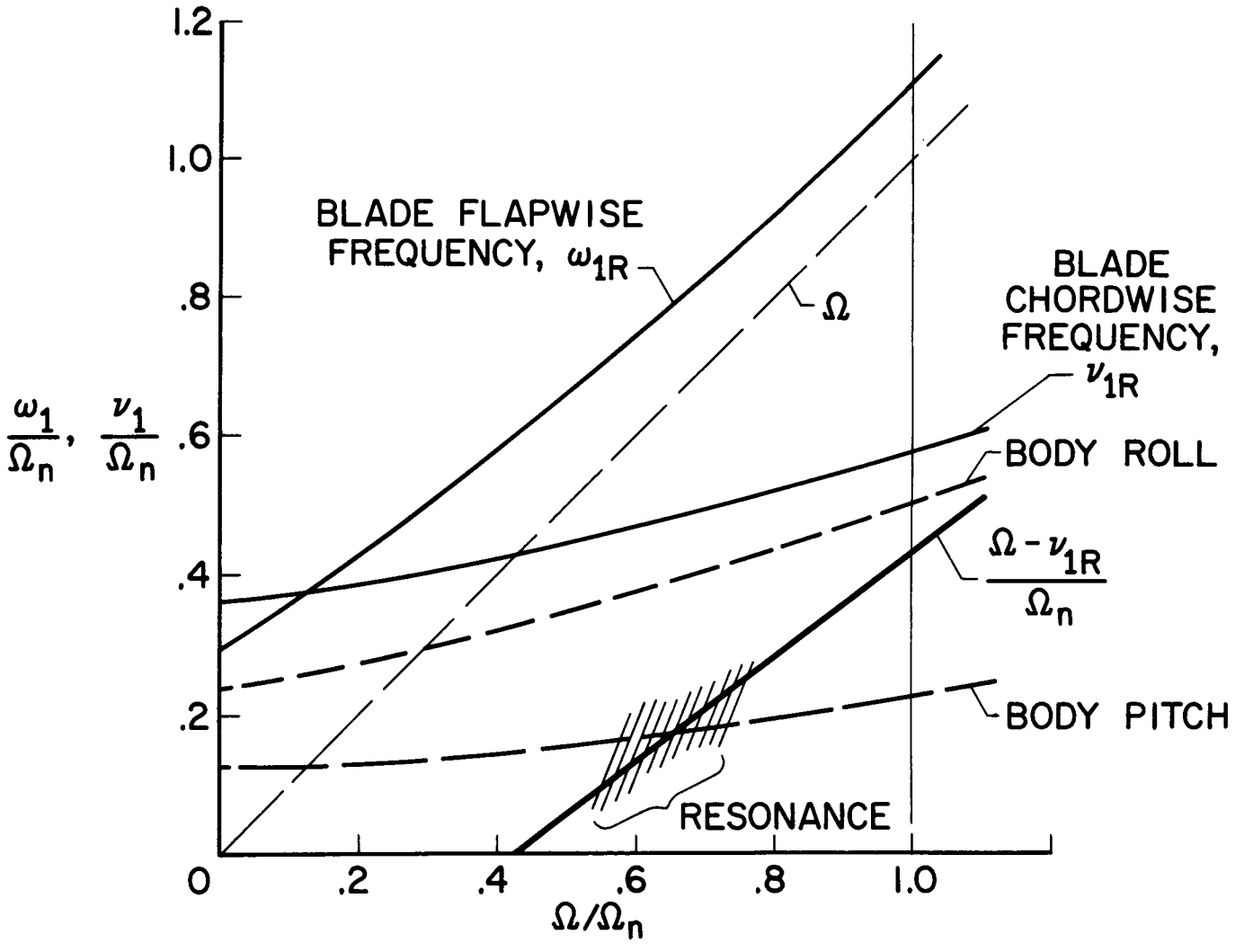

Figure 20.- Ground resonance diagram for reduced chordwise stiffness blade.

Figure 21.- XH-5IN hingeless-rotor research helicopter.